Crust necking of the northeastern South China Sea: Insights from deep seismic data

Lijun Mi[1], Hongdan Deng[2, 3], Mohamed Gouiza [4], Haizhang Yang[1], Qiaoyang Sun[2,3], Siyao Sun[2,3] & Fang Dong[2, 3]

[1] Department of Exploration, CNOOC, Beijing 100010, China.
[2] School of Earth Sciences, Zhejiang University, Hangzhou 310027, China.
[3] Structural Research Centre of Oil & Gas Bearing Basin of Ministry of Education, Hangzhou 310027, China.
[4] School of Earth and Environment, University of Leeds, Leeds, UK.

LM, ; HD, 0000-0002-5546-3884; MG, 0000-0001-5438-2698; HY, ; QS, 0000-0001-8265-9383; SS, ; FD, .

Ital. J. Geosci., Vol. 142, No. 1 (2023), pp. …-…, 12 figs., 1 tab., https://doi.org/10.3301/IJG.2023.06.

Research article

Corresponding author e-mail: denghongdan@gmail.com

Citation: Mi L., Deng H., Gouiza M., Yang H., Sun Q., Sun S. & Dong F. (2023) - Crust necking of the northeastern South China Sea: Insights from deep seismic data. Ital. J. Geosci., 142(1), XX-XX, https://doi.org/10.3301/IJG.2023.06.

Associate Editor: Alina Polonia
Guest Editor: Giacomo Corti

Submitted: 29 May 2022
Accepted: 07 December 2022
Published online: XX December 2022

SOCIETÀ GEOLOGICA ITALIANA
FONDATA NEL 1881 · ENTE MORALE R. D. 17 OTTOBRE 1885

ISPRA
Istituto Superiore per la Protezione e la Ricerca Ambientale

Sistema Nazionale per la Protezione dell'Ambiente

© Società Geologica Italiana, Roma 2023

Accepted manuscript

ABSTRACT

During rifting, continental crust necks, leading to significant thickness reduction in a few tens of kilometres. However, deformations associated with the necking process remain elusive due to few outcrop examples and a lack of seismic data coverage that clearly images crustal architecture at depth. Here we use deep, high-resolution seismic data across a well-developed necking zone in the northeastern South China Sea passive margin to show the structural style associated with the crustal necking. Seismic stratigraphy in the necking domain can be divided into pre-, syn- and post-rift sequences based on the nature of sequence-bounding unconformities and their relation with faults. Seismic expression of continental crust exhibits two types of reflection characteristics – homogeneous upper crust and layered lower crust. The necking domain shows significant thinning that reduced its thickness from ~30 km to less than over 10 km in a distance of about ~50 km and is characterised by seaward removal of layered lower crust, while the homogeneous upper crust thickness remains largely unchanged in thickness. The necking domain is bounded by inner and outer breakaway complexes that define a portion of flexed crust. Crustal flexure is evidenced by progressive tilting of the necking domain that gradually increases the pre-rift sequence dip from 0° to 10°. Within the tilted necking domain, densely-spaced, landward-dipping minor faults and fractures are organised in a domino configuration, implying a top-to-the-continent movement and a simple shear deformation of the whole continental crust. We suggest that the flexed necking domain could be home to fractured reservoir providing that it is effectively sealed by post-rift sequences.

KEY-WORDS: Crust necking, Continental rifting, Crustal-scale faults and fractures, South China Sea.

INTRODUCTION

The last decade of research on modern and fossil magma-poor rifted margins defined distinct structural domains, such as the proximal, necking, distal, outer, and oceanic domains (Péron-Pinvidic & Manatschal, 2009; Mohn et al., 2010; Peron-Pinvidic et al., 2013; Sutra et al., 2013; Osmundsen & Péron-Pinvidic, 2018; Chenin et al., 2021). The proximal domain develops in the initial stage of rifting, when stretching factor β (the amount of thinning, McKenzie, 1978) is low (<2) and deformation is dominated by high-angle normal faults in the upper crust and is accommodated by ductile shearing at depth. The necking domain is characterized by rapid crustal thinning from normal thickness (~30 km) in the proximal domain to ~10 km in the distal domain within a few tens of kilometers. The distal domain represents a stage of hyper-extension where extreme thinning (stretching factor >2) leads to exhumation of subcontinental mantle, as exemplified by the Iberian-Newfoundland conjugate margins in the southern North Atlantic (Minshull et al., 1998; Chian et al., 1999; Whitmarsh et al., 2001). In the magma-rich passive continental margins, the outer domain involves large amount of magma addition that constructs the outer marginal highs, such as the Mid-Norwegian margin (Mjelde et al., 2009; Peron-Pinvidic & Osmundsen, 2016).

The oceanic domain forms following the break-up of continental lithosphere.

Osmundsen & Péron-Pinvidic (2018) suggests that the formation of structural domains is driven by oceanward migration and localization of extensional strain, which is fundamentally controlled by crustal-scale, domain-bounding fault systems or 'breakaway complexes' (Fig. 1). Such structures shape the lateral and down-dip geometry of passive margin and the way continental margins break up (Ranero & Pérez-Gussinyé, 2010; Manatschal et al., 2015; Naliboff et al., 2017; Peron-Pinvidic & Osmundsen, 2018; Lymer et al., 2019; Peron-Pinvidic and Naliboff, 2020; Deng et al., 2020; Gouiza & Naliboff, 2021; Theunissen & Huismans, 2022). The distribution of crustal-scale fault systems reflects substantial spatial-temporal changes in structural, magmatic, and sedimentary evolution during rifting (Peron-Pinvidic & Manatschal, 2019). These faults can be grouped into five principal breakaway complexes (proximal, inner necking, outer necking, distal, and outer), which define distinct structural domains (Fig. 1, Osmundsen & Péron-Pinvidic, 2018). The proximal breakaway complex separates less deformed continent from deformed proximal margin, such as the Mermaid fault system in the inner margin of NW Australia (Deng et al., 2022). The inner and outer necking complexes define the extent of necking domain, which is characterized by a sliver of fault block that shows significant crustal thinning over a short distance (~50 km). The distal breakaway complex marks the boundary of distal margin and is characterized by extreme crustal thinning and/or mantle exhumation. The outer breakaway complex is linked to the continental lithosphere breakup, which involves igneous addition with a varying magmatic budget among different margins (Strachan et al., 2013; Harkin et al., 2019; Sun et al., 2019a; Tugend et al., 2020; Karner et al., 2021; Pindell & Heyn, 2022).

Among all the rift domains, the necking domain marks a stage of sharp change in basement topography, strain distribution, thermal state, style of rifting, and sedimentary basin formation in continental margins (Braun & Beaumont, 1989; Lavier & Manatschal, 2006; Mohn et al., 2012; Chenin et al., 2017, 2018, 2020). In the necking domain, diffuse deformation become more localized, allowing for hyper-extension of continental lithosphere. Recent research on crustal necking has greatly benefited from high-resolution seismic reflection dataset across many rifted system worldwide, such as the South Atlantic conjugate margins (Stica et al., 2014; McDermott et al., 2015; Paton et al., 2017; Reuber et al., 2019; Karner et al., 2021; Chauvet et al., 2021; Sapin et al., 2021), the east and west Indian margins (Harkin et al., 2019; Geoffroy et al., 2020; Nemčok et al., 2022), the east African margin (Sinha et al., 2019; Haji Hassan et al., 2020; Mortimer et al., 2020), the Gulf of Mexico margins (Pindell et al., 2014; Izquierdo-Llavall et al., 2022), and the northern North Atlantic margins (Osmundsen & Ebbing, 2008; Osmundsen & Péron-Pinvidic, 2018; Cawood et al., 2021). Detailed deformation in the necking zone has also been revealed in fossil Alpine Tethys margin (e.g. Mohn et al., 2012; Ribes et al., 2020). Studies suggest that the development of continental necking may be controlled by inherited crustal-scale weaknesses (Huismans & Beaumont, 2007; Chenin & Beaumont, 2013; Wenker & Beaumont, 2018) and thermal weakening (Callot et al., 2002; Geoffroy, 2005; Franke, 2013; Geoffroy et al., 2015).

In addition, the necking domain represents a transition from continental shelf to deep-water rifted margins, where many frontier areas of hydrocarbon exploration worldwide attracted the interest of industry and researchers (Unternehr et al., 2010; McClay & Hammerstein, 2020). Despite all these attempts to understand the necking zone, only a few studies show clearly the associated deformation, because most necking domains are (partly) deeply-buried under thick sedimentary units and/or lava piles (e.g. Karner et al., 2021; Chauvet et al., 2021; Pindell & Heyn, 2022; Deng et al., 2022). In addition, the lack of high-resolution seismic data makes it difficult to constrain crustal architecture of these domains. Many of the previous studies merely rely on widely-spaced regional cross-sections, which makes it difficult to constrain the three-dimensional strain distribution. Therefore, the significance of necking domain in term of hydrocarbon exploration remains largely underexplored.

In this study, we present new, high-resolution, closely-spaced deep seismic data in order to resolve the crustal-scale faults and fractures in a well-developed necking zone in the northern part of the northeastern South China Sea (Figs. 1 and 2). We integrate seismic reflection data and forward gravity modelling to constrain the crust properties and to validate our interpretation. Based on

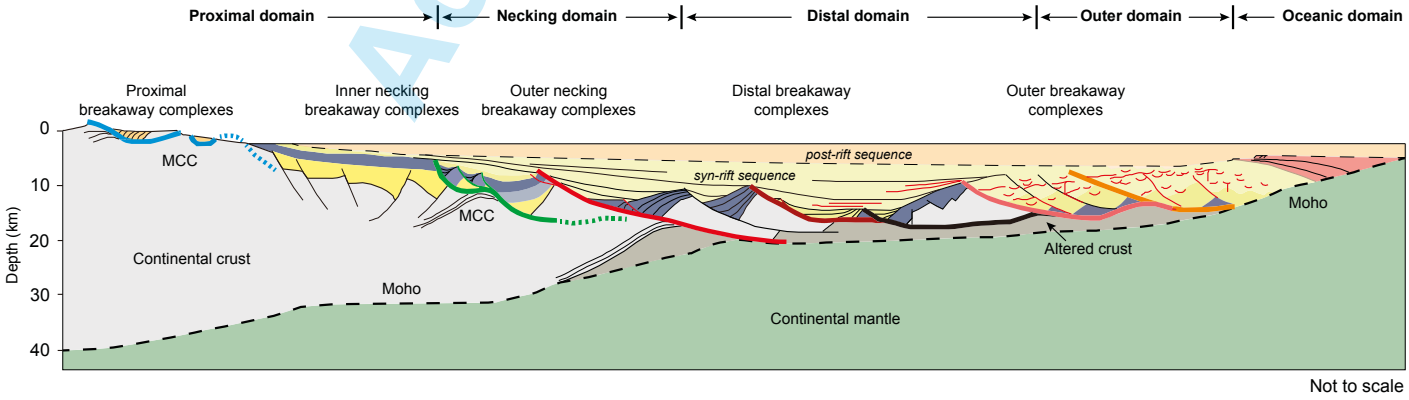

Fig. 1 - Schematic diagram showing crustal-scale fault complexes in different domains of a rifted continental margin (from Osmundsen & Péron-Pinvidic, 2018). MCC: metamorphic core complex.

Accepted manuscript

these new data, we discuss the characteristics of necking domain deformation with particular focus on the fractures and extensional faults in the upper and lower crusts. The lateral and down-dip changes in deformation styles provide the first- and second-order observations of the necking domain. Our proposed model of the northeastern South China Sea sheds new lights on the evolution of the margin itself and provides important implications for petroleum systems evaluation in the necking domain.

GEOLOGICAL SETTING

Continental rifting of the South China Sea

The South China Sea (Fig. 2a) is one of the largest marginal seas in the western Pacific. It formed through continental breakup of the South China and experienced multiple phases of widespread magmatism since Early Permian (Li et al., 2012, 2018; Mai et al., 2018; Suo et al., 2019; Cai et al., 2019; Cui et al., 2021; Zhu et al., 2021; Hennig-Breitfeld et al., 2021). In the early Late Cretaceous (~100 Ma), rollback of Paleo-Pacific plate initiated continental extension in the South China Sea and adjacent areas (Li et al., 2014; Zheng & Dai, 2018; Zhang et al., 2019; Wu et al., 2020). Continued extension in the early Cenozoic (~58 Ma) in response to northward subduction of the Proto-South China Sea resulted in lithospheric stretching and thinning that eventually led to final continental breakup in the early Oligocene (~32 Ma) (Lin et al., 2003; Huang et al., 2005; Savva et al., 2014; Franke et al., 2014; Sun, 2016; Sibuet et al., 2016; Xie et al., 2019; Wang et al., 2019; Li et al., 2020; Zhu et al., 2021). Seafloor spreading of the South China Sea ceased in the Middle Miocene (~16 Ma) and then the oceanic crust was subjected to eastward subduction along the Manila trench in the Pliocene (~5 Ma) (Lester et al., 2013; Eakin et al., 2014, 2015; Xie et al., 2019; Chiu et al., 2021).

Cenozoic rifting of the South China Sea created a wide and distributed continental margin that reaches up to 1,000 km in width with a crustal architecture showing marked along-strike and down-dip geometrical variations (Savva et al., 2014; Franke et al., 2014; Gao et al., 2016; Pubellier et al., 2018; Bai et al., 2019; Ding et al., 2020; Deng et al., 2020; Wen et al., 2021; Li et al., 2021; Chang et al., 2022). The distributed deformation is mostly controlled by detachment faults and magmatism and developed in a high geothermal condition (Larsen et al., 2018b; Nirrengarten et al., 2019; Sun et al., 2019a; Ding et al., 2020; Zhang et al., 2021a; Zhao et al., 2021a; Chao et al., 2021). Recent research based on Integrated Ocean Drilling Program (IODP) in the distal, outer, and oceanic domains of the South China Sea have made significant progress in the understanding of the continental margin formation and evolution (Lin et al., 2019; Huang et al., 2019; Sun et al., 2019a; Wang et al., 2019; Zhao et al., 2019). These studies suggest that the rifted continental margin is neither a magma-poor nor a magma-rich margin and is more likely an intermediate margin that combines characteristics from both (Yeh et al., 2012; Larsen et al., 2018b).

The rifted margin of the South China Sea shows a wide proximal domain that reaches up to 400 km and multiple necking zones (Gao et al., 2015, 2019; Le Pourhiet et al., 2018; Yang et al., 2018; Cameselle et al., 2020). The necking zones are commonly bounded by crustal-scale detachment faults (Zhao et al., 2018; Wang et al., 2018; Liang et al., 2019; Xie et al., 2019; Fang et al., 2022). In the distal domain, large amount of magmatic additions are associated with detachment faults that thinned the continental crust and led in places to exhumed middle and lower crust (Sun et al., 2019b; Deng et al., 2020; Zhang et al., 2021b). Apart from the down-dip changes of the structural domain, geophysical data, such as Ocean Bottom Seismic (OBS), indicate the existence of a high-velocity layer underneath the distal domain, implying the presence of magmatic underplating in the lower crust (Pin et al., 2001; Wang et al., 2006, 2020; Zhao et al., 2010; Lester et al., 2014; Wan et al., 2017, 2019; Xia et al., 2018; Cheng et al., 2021; Chiu et al., 2021).

Northeastern South China Sea and "failed rift"

Continental rifting of the South China Sea formed a distributed, highly-extended sub-basins in the rifted margins (Cameselle et al., 2020). The northeastern South China Sea is one of these sub-basins that shows distinct bathymetric expression (Fig. 2a). It is bounded by the continental shelf to the north, the Manila Trench to the east, and the oceanic basin to the south, covering an area of 300*400 km^2. The eastern part of the margin has been partially subducted along the Manila Trench (Lin and Watts, 2002; Chang et al., 2012; Eakin et al., 2014; Chiu et al., 2021; Sibuet et al., 2021). The northeastern South China Sea shows rugged features on the seafloor, such as NE-trending post-rift magmatic edifices that are clearly identifiable from the bathymetry map (Fig. 2a, Lester et al., 2014; Sibuet et al., 2016; Xu et al., 2022).

The nature of the northeastern South China Sea has been debated since early 2000s. Based on the distribution of magnetic anomalies, Hsu et al. (2004), Tsai et al. (2004), and Yeh et al. (2010) suggest that the entire northeastern South China Sea is made of oceanic crust. However, newly-acquired reflection/refraction seismic data in 2009 suggest that the crust is rather of a transitional nature, exhibiting characteristics of the continental-ocean transition zone (Yeh et al., 2012). More recent works suggest that the northeastern South China Sea has a highly-extended continental crust that has been heavily intruded and modified by magma (Sibuet et al., 2016, 2021; Wan et al., 2019; Zhang et al., 2021c; Chiu et al., 2021).

In the north of the northeastern South China Sea, between 22° and 21° N, continental crust has been significantly thinned down to ~5 km, where the highly stretched basin failed to progress to breakup (Fig. 2b and Fig. 3, Nissen, 1995; Nissen et al., 1995; Yeh et al., 2012; McIntosh et al., 2014; Lester et al., 2014; Liu et al., 2018; Cheng et al., 2021; Zhang et al., 2021c; Chiu et al., 2021) and has been named as "failed rift" by McIntosh et al., (2014). The "failed rift" has a width of ~100 km and a length of ~150 km, with the eastern part being subducted. The "failed rift" is characterized by a negative magnetization zone that trends NE (Yeh et al., 2012). It is buried beneath the base of continental slope and has experienced large amount of stretching (β=7.5) along the rift axis (McIntosh et al., 2014). To the south and north of the "failed rift", crust thickness is 10-14 km and 30 km, respectively. Recent studies indicate that the "failed rift" developed as part of the northern South China Sea margin that evolved from early Paleogene to late Eocene (Lester et al., 2014).

Accepted manuscript

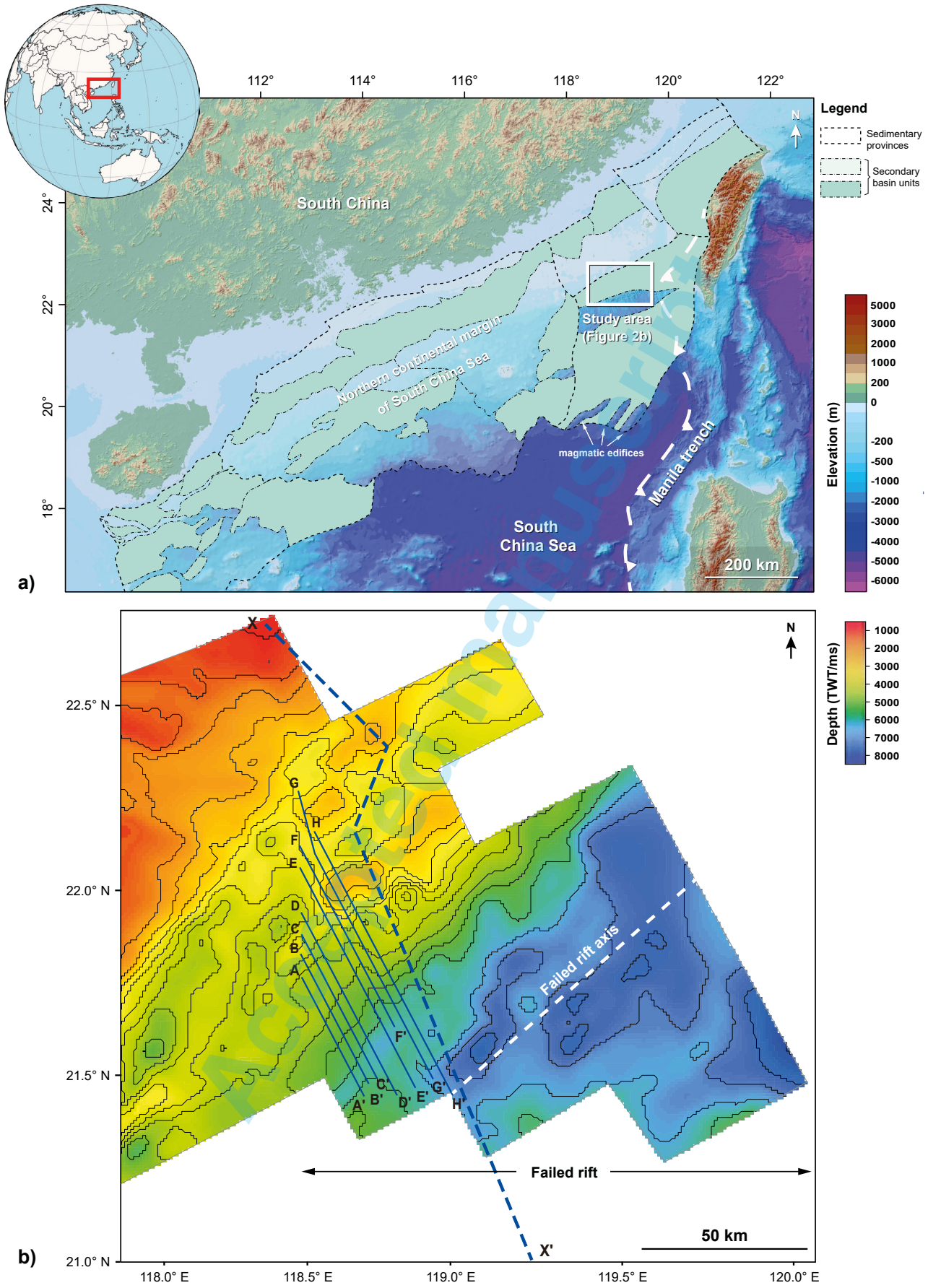

Fig. 2 - (a) Topography and bathymetry map of the northern South China Sea margin and the adjacent areas showing the location of the study area. Note the magmatic edifices in the south of the northeastern South China Sea. (b) Time structure map of top basement (S2) of the west part of northern South China Sea showing the location of seismic lines used in this study (see map location in Fig. 1). The "failed rift" in the northeastern South China Sea trend NE. Note that rapid change of depth of the top basement in the necking domain (contour interval = 500 ms) in a distance of about 50 km.

Accepted manuscript

DATASETS AND METHODS

Datasets

Seismic reflection data has been an indispensable tool for the investigation of continental deformation at depth (Barazangi & Brown, 1986), as it is by far the best to image structural fabrics in deep basement with the highest possible resolution (e.g., Allmendinger, 1983; Allmendinger et al., 1987a; Dong et al., 2013; Zhang et al., 2022). Our work integrates the latest, high-quality seismic data from industry and academia (Fig. 2b). The industry data were recently acquired in 2019 by the China National Offshore Oil Corporation (CNOOC). The academic data were collected in 2009 by TAiwan Integrated Geodynamics Research (TAIGER) project (Yeh et al., 2012). The latest high-resolution seismic reflection data, which are much improved than the old datasets (e.g., Sibuet et al., 2002; Lin et al., 2003; Tsai et al., 2004; Li et al., 2007; Yeh et al., 2010), enable us to map the crustal architecture and the extent of the necking domain in unprecedented detail. All these datasets have a record depth of 12-14 s TWT and are of good quality and resolution at depths. Seismic line spacing is ~4 km and most of the lines are 50-100 km long, covering the entire necking domain along the dip of the northeastern South China Sea (Figs. 2). The data from CNOOC were acquired using one streamer and one source. They have a record depth of 12 s (TWT) and a sample rate of 2 ms. The data from TAIGER project were acquired by one airgun array (BOLT: 1,500 LL), fired every 50 m at 2,000 psi. The total volume used was 6,600 in^3, towing at a depth of 8 m throughout the survey. The data were collected using a hydrophone stream, 5,850 m in length, containing 468 channels.

The seismic data has a dominant frequency in seabed of ca. 60 Hz and the average interval velocity of ca. 1500 m/s; these values for frequency and velocity yield a vertical resolution of ca. 6.25 m. A lower (ca. 18 Hz) dominant frequency and a faster average interval velocity (ca. 4000 m/s) in the Mesozoic unit (Fig. 4) yield a vertical resolution of ca. 55.6 m. The dominant frequency content is about 12 Hz and the interval velocity increases from 6000 to 7500 m/s across the middle-lower crust. Hence, the vertical resolution of the basement rocks is calculated at 125-156.3 m.

Seismic interpretation

Seismic interpretation was performed using Geoframe 2012 software. We picked five key horizons; these are the Moho, the base of pre-rift sequence boundary (S1), the base of syn-rift sequence boundary (S2), the base of post-rift sequence boundary (S3), and seabed (Fig. 4). Seismic Moho is a high-amplitude reflector of high acoustic contrast. This reflection has been identified independently by OBS data and has been calibrated to our study (e.g. Lester et al., 2014; Chiu et al., 2021). The stratigraphy of northeastern South China Sea was correlated to the detailed studies of southwest Taiwan and adjacent areas (Lin et al., 2003, 2021; Liao et al., 2016). We followed the Cenozoic stratigraphic framework established by Huang et al., (2012) and Lin et al., (2003), which suggest that syn-rift stratigraphy started at 58 Ma and ends at 37-32 Ma. Therefore, S2 and S3 horizons can be correlated to Tg (top basement boundary, ~56 Ma) and T70 (top syn-rift sequence boundary, ~32 Ma), respectively, in other parts of the South China Sea margins (Xie et al., 2019).

We picked major faults to show lateral and downdip changes in deformation style and fault geometry across the necking domain. In addition, we performed detailed interpretation of intrabasement reflections to illustrate the structural fabrics configuration using Adobe Illustrator 2022 (Fig. 4). During the interpretation, we firstly identified acquisition or processing artifacts. These artifacts are landward-dipping, low-amplitude reflectors that are persistently present both in the crust and in the subcontinental mantle (Fig. 4). They have constant reflection pattern and shows little changes in reflection strength. The structural fabrics, however, show distinct characteristics that have higher reflection amplitude with variable geometries.

Depth conversion and gravity modelling

Depth conversion and forward gravity modelling were performed on a regional section X-X' across the northeastern South China Sea (location in Figs. 2b) to validate the interpretation of continental crust. For depth conversion, we adopted constant interval velocities for the water column (1500 m/s), the post-rift sediments (2,450 m/s), the syn-rift sediments (3,850 m/s), and the continental crust (6,250 m/s). We did not separate the pre-rift Mesozoic sediments from the crystalline basement (Fig. 3c-d) because the Mesozoic sedimentary rocks are relatively thin, which would have a limited effect on the depth conversion of the overall crustal thickness. Seismic velocities were derived from recent seismic refraction studies in the northeastern South China Sea (Table 1; Wan et al., 2017; Xia et al., 2018).

Table 1 - Seismic velocities and densities in the South China Sea

	Seismic velocities (m/s)			Densities (g/cm^3)		
	Wan et al. (2017)	Wan et al. (2019)	***This study***	Wan et al. (2017)	Xia et al. (2018)	***This study***
Shallow (post-rift) sediments	2000 – 4000	1700 – 3200	***2450***	1.91	2	***2.1***
Deep (pre-and syn-rift) sediments	4000 – 5000	3500 – 4200	***3850***	2.53		***2.5***
Upper crust	5500 – 6400	5500 – 6400	***6250***	2.68 – 2.76	2.65	***2.85***
Lower crust	> 6400	6400 – 6800		2.81 – 3.18	2.85 – 3	
Upper mantle				3.32	3.2	***3.3***

Accepted manuscript

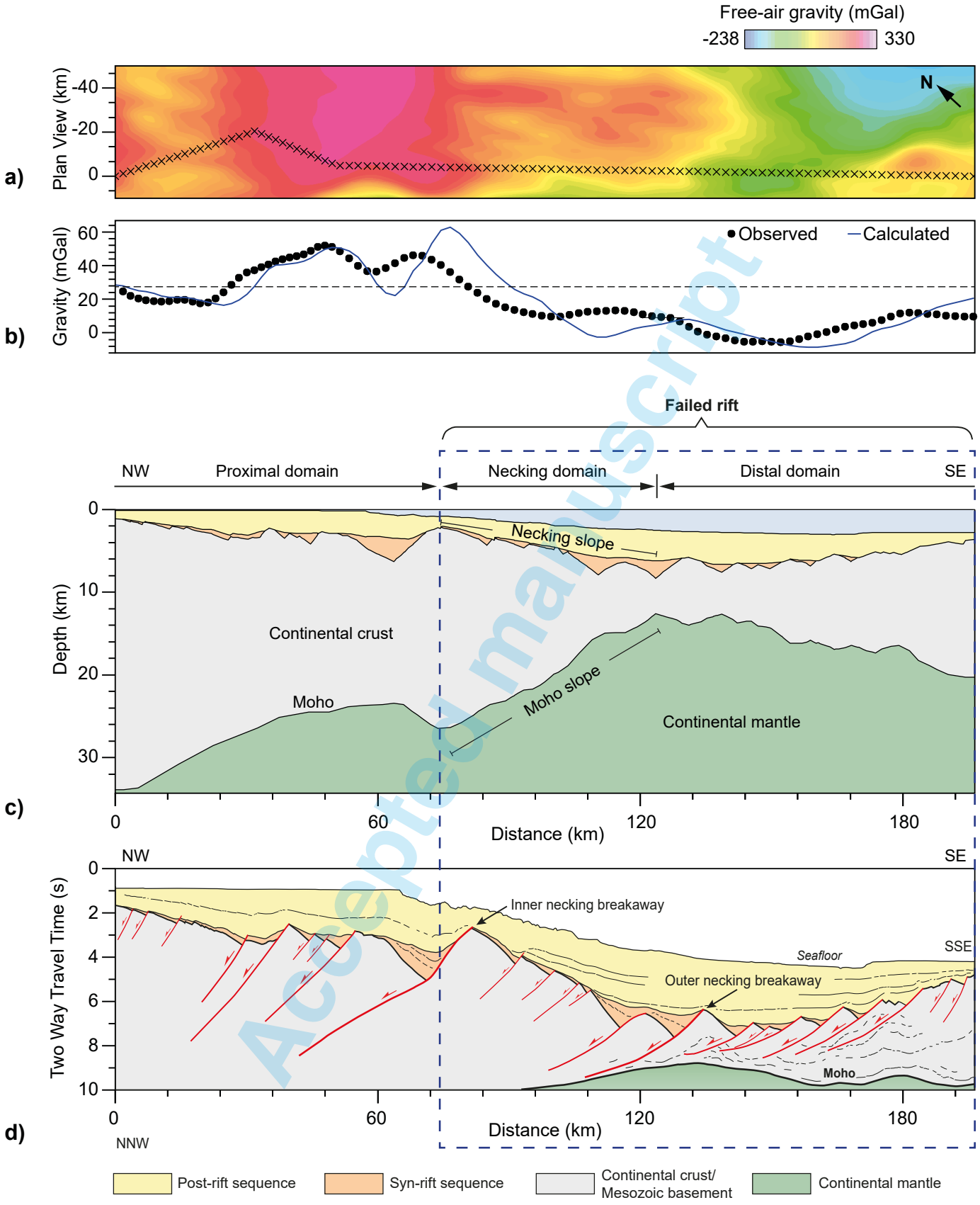

Accepted manuscript

Fig. 3 - (a) A strip of free air gravity along the seismic transect X-X' in the northeastern South China Sea (section location in Fig. 2). (b) Comparison of observed (thick dotted line) and modelled (solid line) gravity along seismic transect X-X'. (c) Depth-converted section X-X' showing the crustal architecture from proximal to distal domains. Note that the necking zone shows rapid thickness change from 25 km to <10 km across the necking zone. (d) Time section showing crustal architecture. Note that the necking domain is bounded by a series of landward dipping extensional faults and the domain-bounding faults are inner and outer breakaway complexes.

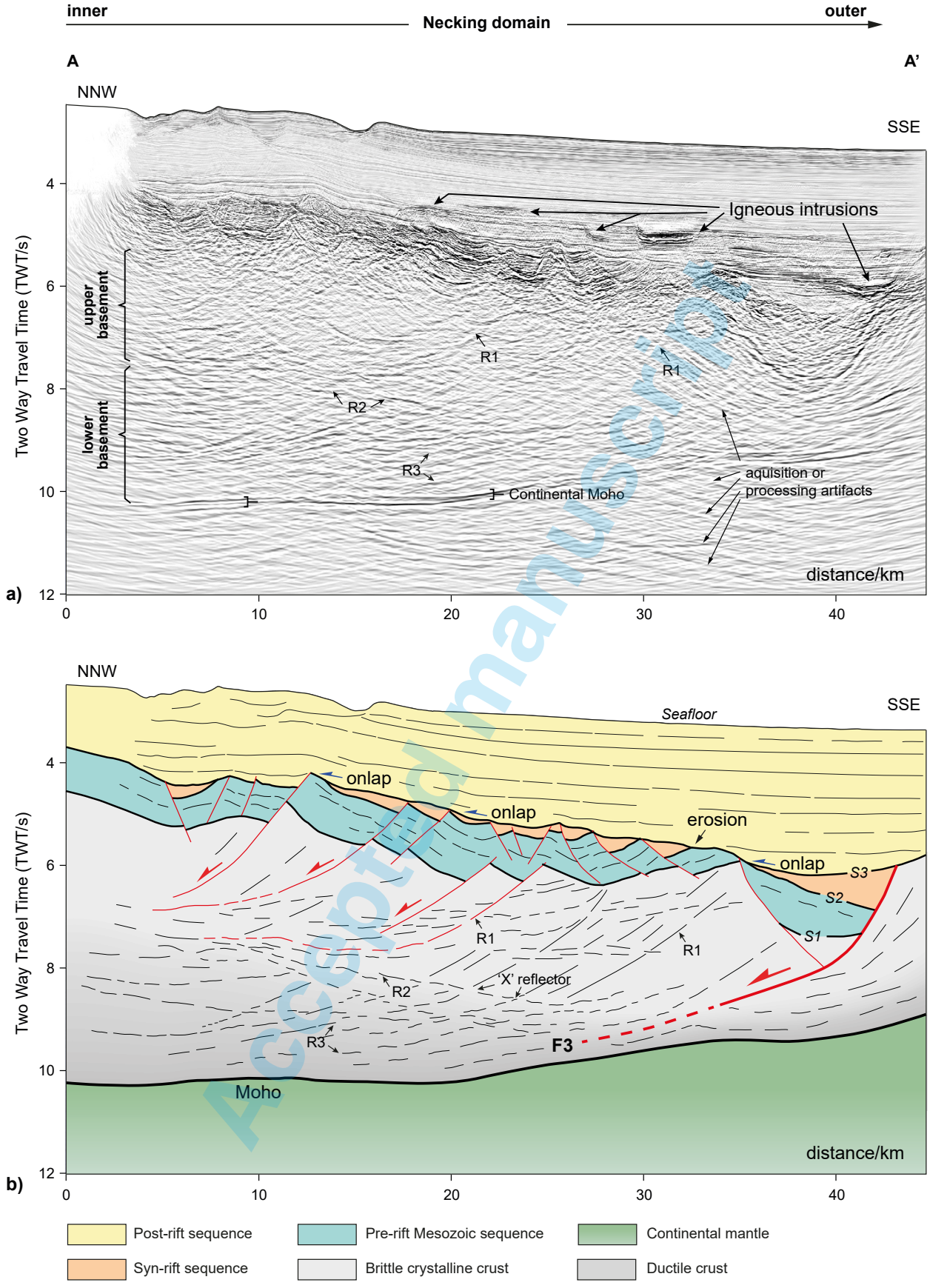

Accepted manuscript

Fig. 4 - Uninterpreted seismic section A-A' (a) and its interpretation (b) showing detailed deformation of the necking domain (section location in Fig. 2). F3 is the outer breakaway complex. S1, S2, and S3 are three unconformities that separate the top-basement, pre-rift, syn-rift, and post-rift sequences. R1, R2, and R3 are three types of reflectors in the basement. Note that the homogenous basement in the upper part of the necking domain is dominated by land-ward dipping reflections (R1) that are interpreted as fractures. R2 is sub-parallel to the top basement. R3 is sub-parallel to the seismic Moho. In the post-rift sequence, the high-amplitude, saucer-shaped and step-like reflections are interpreted as igneous intrusions.

The forward 2D gravity modelling was undertaken in Geosoft Oasis Montaj software, which assumes a layered-earth model (GM-SYS profile modelling; Pouliquen et al., 2017), in combination with public satellite free-air gravity data. The seismic horizons, picked along seismic line X-X', were used to constrain the margin architecture and to define different stratigraphic packages and crustal domains. Thus, constant densities were given to water (1.03 g/cm^3), syn-rift sediment (2.1 g/cm^3), post-rift sediment (2.5 g/cm^3), continental crust (2.85 g/cm^3), and upper mantle (3.3 g/cm^3). These density values are in agreement with densities calculated from refraction P-velocities in the South China Sea (Table 1; Wan et al., 2017; Xia et al., 2018).

NECKING DOMAIN OF THE NORTHEASTERN SOUTH CHINA SEA

The necking domain in the study area is defined by its thickness change that reduces from ~30 km in the north to <10 km in the south (Fig. 3c). The change in crust thickness is associated with faults that we defined as inner and outer necking breakaway complexes (Fig. 3d). Observations of necking domain structures are based on a regional seismic section X-X' and seven short seismic sections that show the structural and stratigraphic architecture (Fig. 2b).

Stratigraphy

Previous work in the northeastern South China Sea suggested that there was no syn-rift sequence associated with the Cenozoic rifting (e.g., Lin et al., 2003). This is however largely due to poor seismic quality that was not able to resolve the deeper part of the basin. In this contribution, high-resolution seismic data provide clear image of the sedimentary basin and underlying basement (e.g., Figs 4-5), which allows us to re-evaluate and to re-define pre-, syn- and post-rift sequences based on their stratigraphic architecture and associated faults. The pre-, syn-, and post-rift sequences are bounded by basement and Mesozoic/Cenozoic boundaries (S1-S2 interval), syn- to post-rift unconformities (S2-S3 interval), and post-rift unconformity to seabed (S3-seabed), respectively (Fig. 4).

The pre-rift megasequence shows layered, sub-parallel, and continuous reflection overlying homogeneous, low-amplitude basement rocks (Figs. 4-5). It is bounded at the top by S2 and at the bottom by S1, has a thickness of ~1 s (TWT) or 1-1.5 km, and consists of low- to medium-amplitude reflections in the bottom and high-amplitude reflections in the middle and upper sections. The sedimentary package is offset by Cenozoic faults and shows little change in thickness, which therefore could be used as a stratigraphic marker for upper crust deformation. Wells in the northeastern South China Sea margin indicate that the layered reflection are Mesozoic strata (e.g., Li et al., 2008; Hao et al., 2009; Yang et al., 2012; Zhou et al., 2021; Fan et al., 2022). Figure 5 shows that the Mesozoic beddings show a dip increases from 0° in the inner necking domain to 10° in the outer necking domain. The increase in bedding dip of pre-rift Mesozoic strata, albeit smaller, can be observed in other sections (Figs. 6-8). More pronounced bedding rotation is observed in Figures 9-10. The dip gradient for the necking domain is ~0.33 °/km in section B-B', ~0.22 °/km in section E-E', and ~0.2 °/km in section F-F' (Figs. 5, 8 and 9).

The syn-rift megasequence is distributed across the necking domain. It has the maximum thickness of <1 s (TWT) or 1-1.5 km in the inner and outer domains, bounded by domain boundary faults (Fig. 3d). On the necking slope, growth wedges are small (<0.1-0.2 s TWT) and are mainly controlled by small-scale faults (Figs. 4-6). Seismic reflection of the growth strata is characterised by low-amplitude, continuous, and divergent reflections, bounded by horizon S2 at the bottom and horizon S3 at the top. Above S2, syn-rift growth wedges are rarely connected and are distributed across the necking domain. In many places, these growth wedges are separated by faults and fault-bounded blocks or have been eroded after the deposition of the growth strata (e.g., Fig. 4).

The post-rift megasequence is bounded at the bottom by S3 and at the top by the seabed. It has a maximum thickness of 3 s (TWT), about 4-6 km (Figs. 4-7). In the down-dip direction, this sedimentary package thickens towards the south. The change in thickness in down-dip direction can also be seen in the structural map of S2, which shows progressive deepening of the base Cenozoic surface towards the rift axis (Fig. 2b). In the strike direction, the post-rift sequence thickens towards the northeast. Seismic reflection of the post-rift strata is dominated by medium- to low-amplitude continuous reflections. Figure 5 shows that the lowest or oldest post-rift sequence develops in the outer necking domain and younger sediments gradually fill the higher or inner parts in the north. In the post-rift megasequence, we can see high-amplitude reflections that show saucer-shaped, stepping geometries in the places where the necked crust is thin (Figs. 4, 5 and 7). However, this reflection pattern is unevenly distributed and can only be observed in the western part of the rift.

Basement

The basement of the continental crust in the necking domain is characterised by low-amplitude, homogeneous reflections in the upper level and low- to medium-amplitude, layered reflections in the lower level (Fig. 4). The homogeneous basement has been overprinted by landward-dipping reflections (R1), whereas the layered basement is dominated by converging reflections (R2 and R3) that are subparallel to the top basement and the Moho, respectively.

Homogeneous upper basement

The homogeneous basement forms the upper and middle parts of the continental crust and is characterized by low-amplitude, discontinuous reflections that have a thickness of 2-3 s (TWT) or 6-9 km (Figs. 4 and 7). The homogeneous basement is overlain by the Mesozoic strata, which cover all parts of the necking domain, implying that the upper part of the basement is intact. The homogeneous basement has an unchanged thickness and is bounded at the top and the bottom by S1 and R2, respectively. R2 is characterized by a series of semi-continuous reflections that dip towards the ocean direction at a shallow angle.

Accepted manuscript

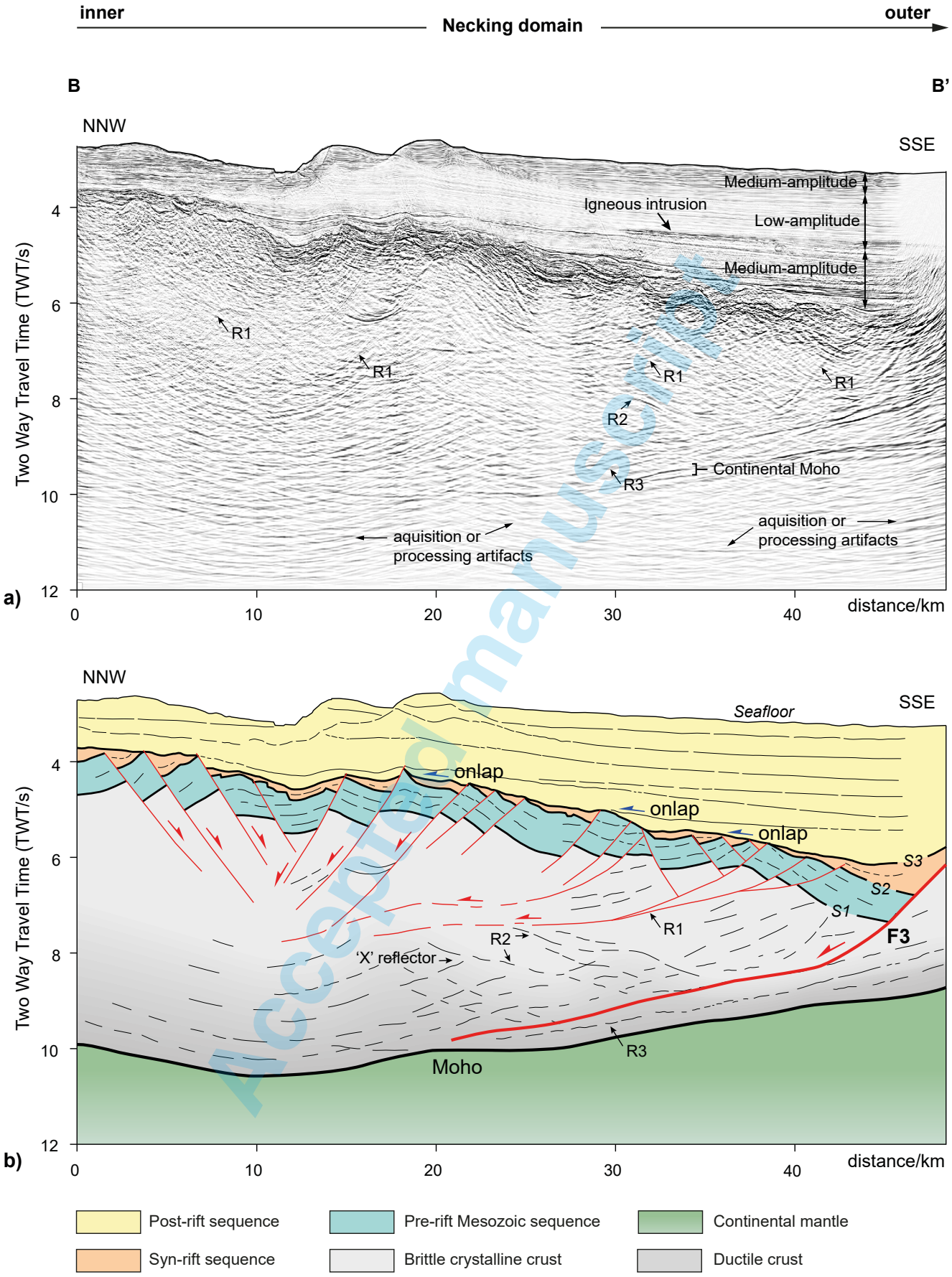

Accepted manuscript

Fig. 5 - Uninterpreted seismic section B-B' (a) and its interpretation (b) showing detailed deformation of the necking domain (section location in Fig. 2). F3 is the outer breakaway complexes. S1, S2, and S3 are three unconformities that separate the top-basement, pre-rift, syn-rift, and post-rift sequences. R1, R2, and R3 are three types of reflectors in the basement. Note that seismic character of post-rift sequence is featured by medium-, low-, and medium-amplitude reflections. Stratigraphic onlaps over the S1 show the infill pattern of the post-rift sequence.

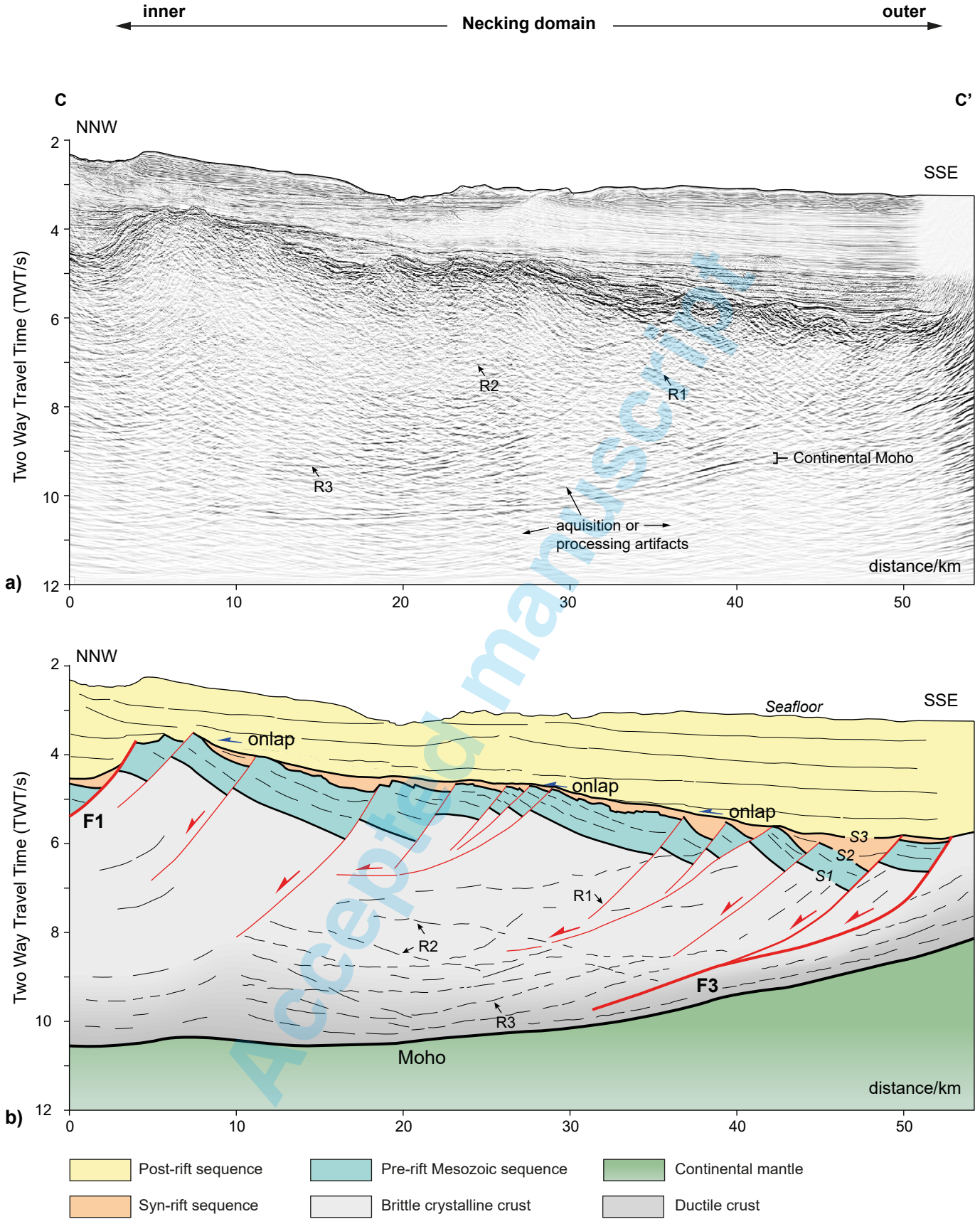

Accepted manuscript

Fig. 6 - Uninterpreted seismic section C-C' (a) and its interpretation (b) showing detailed deformation of the necking domain (section location in Fig. 2). F1 is the inner breakaway complex and F3 is the outer breakaway complexes. S1, S2, and S3 are three unconformities that separate the top-basement, pre-rift, syn-rift, and post-rift sequences. R1, R2, and R3 are three types of reflectors in the basement. Note that the outer breakaway complex consists of a splay fault in the hangingwall of F3, which soles on the main fault (F3) and bifurcate upwards into a separate fault. In immediate footwall of F1, upper basement shows symmetric reflectors.

It is sub-parallel to the top basement and is the detachment level of some landward-dipping reflections (R1). Rapid thinning of the homogeneous basement is observed in the outer domain, where it is bounded by a landward-dipping detachment fault. The footwall of the detachment fault is layered lower basement that are exhumed to shallower depth, while the upper basement has been displaced by outer necking breakaway complex (Fig. 3d).

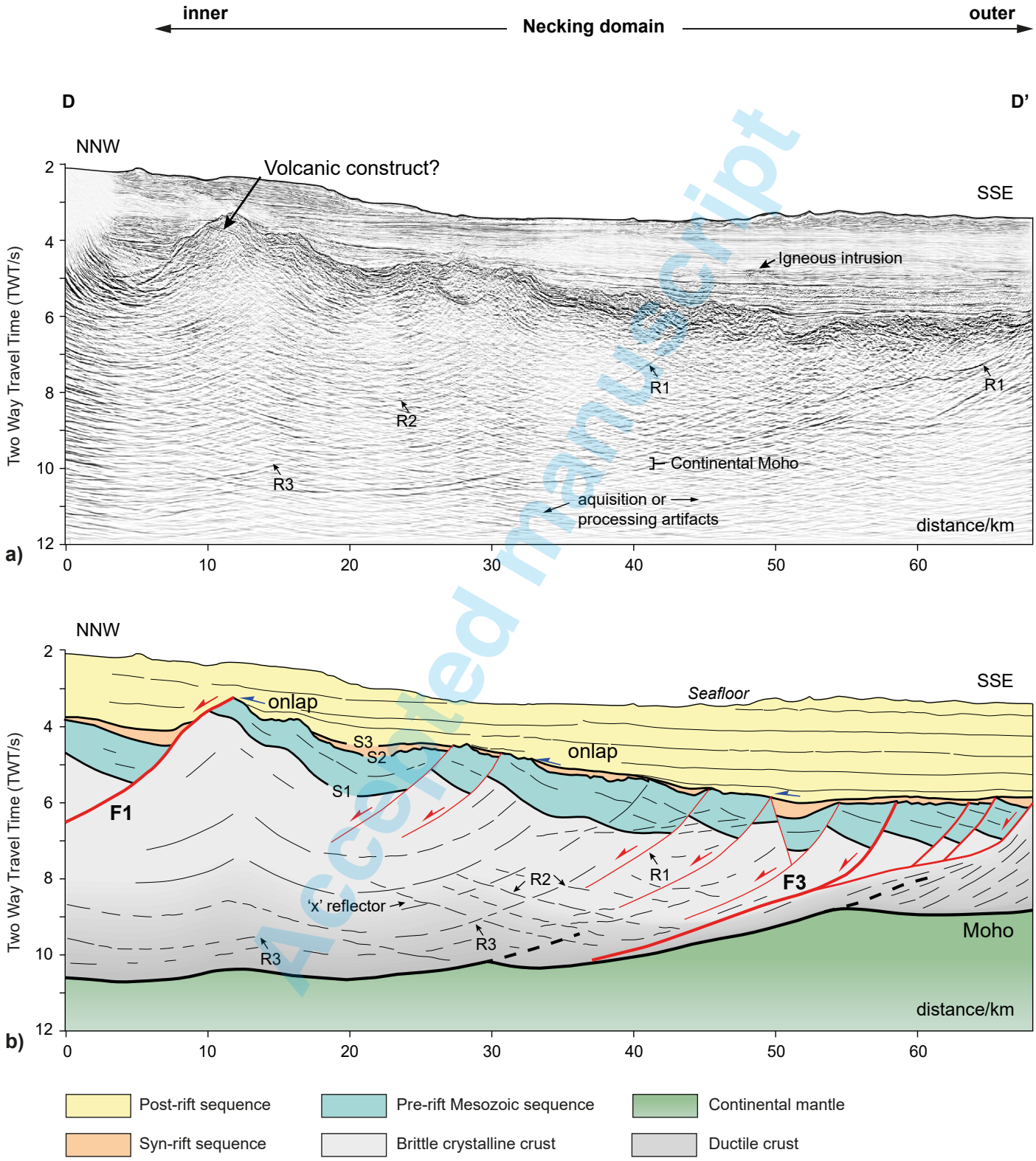

Accepted manuscript

Fig. 7 - Uninterpreted seismic section D-D' (a) and its interpretation (b) showing detailed deformation of the necking domain (section location in Fig. 2). F1 is the inner breakaway complex and F3 is the outer breakaway complex. S1, S2, and S3 are three unconformities that separate the top-basement, pre-rift, syn-rift, and post-rift sequences. R1, R2, and R3 are three types of reflectors in the basement. Note that in the immediate footwall of F1, upper basement shows symmetric reflectors. F3 consists of four fault splays; they sole into the lower part of the crust.

Layered lower basement

The layered basement forms the lower part of the continental crust and is bounded by R2 on the top and by the reflective Moho at the bottom (Fig. 4). The reflection character of layered basement is low- to medium-amplitude and is dominated by semi-continuous reflections. The spacing of layered reflections increases downward and reaches the maximum near the seismic Moho. Most of the landward-dipping reflections (R1) in the homogeneous basement sole into the layered basement and some may reach down to the Moho (e.g., Figs. 5, 7, 9, 10). The maximum thickness of the layered lower basement is observed in the inner necking domain, where it has a thickness of 3 s (TWT) or 9 km; The minimum thickness is observed in the outer domain, where it has a thickness of less than 1 s (TWT) or 3 km (Figs. 7-10). In the down-dip direction, the layered basement become more pronounced in the outer domain compared to that of the inner domain. In the outermost part, the overlying homogeneous basement becomes absent in most of the sections, while layered reflections becomes the dominant. Figures 8-10 show that the layered basement have a thickness of ~2 s (TWT) in the north and ~1 s (TWT) in the south.

Seismic Moho

The seismic Moho consists of one or several high-amplitude reflections that separates the layered lower crust above and homogenous low-amplitude mantle below. The reflection is very clear in the southern or outer parts of the necking zone, where the crust is significantly thin; whereas the reflection is less obvious in the northern or inner parts of the necking domain, where the crust is thick (Figs. 5-10). The seismic Moho has a maximum depth (10-11 s, TWT) in the inner necking domain and it gradually shallows up towards the outer domain at 8-9 s (TWT). In Figure 3, the Moho reflection in the central part of the "failed rift" bows upward to 8 s (TWT) and dips towards the northern and southern margins, exhibiting a symmetrical geometry around the rift axis. Moho slope in the necking domain is about 20° (Fig. 3c). Although the seismic Moho depth decreases steadily from the south to the north, we observe locally elevated Moho beneath the inner necking breakaway F2, where we interpret the igneous intrusion (e.g., Figs. 6-7). In Figures 7 and 9, we can also see two places of locally elevated Moho that are linked to a high-amplitude reflection in the lower part of the layered basement. In addition, the thickness of the seismic Moho changes across the necking domain. In Figure 4, the seismic Moho consists of 4-5 reflections that are 100-200 ms thick; whereas in Figure 8, the seismic Moho consists of one reflection only.

Faults and fractures

Faults and fractures are interpreted in the basement of the necking domain based on its reflection patterns. We can identify at least three types of reflections (R1-R3) that show persistent reflection patterns in all seismic sections (Fig. 4). R1 are reflections mainly observed in the upper and lower parts of the crystalline basement. They can be traced across the homogeneous crust and detach into the layered lower crust, showing semi-continuous reflections that are predominantly dip towards the continent (Fig. 10). They shallow towards the outer necking zone, showing tilting of reflections in a domino-style fashion. Further upward, we can see that the landward-dipping reflections are linked with densely-spaced top-basement faults that offset the pre-rift sedimentary succession (Figs. 5-10). The displacement along the faults, which can be measured based on the offset of pre-rift sequence, is mostly less than 1 km within the necking domain. R2 and R3 are reflections in the lower parts of the basement; they converge towards the outer domain. Both R2 and R3 are detachment levels that R1 soles onto, although many R1 reflections can be tracked across the R2 reflection. In this case, the cross-cutting of R1 and R2 shows 'x' reflection in the lower basement (Figs. 4-5, 7-8, and 10).

The identification of breakaway complexes is constrained by crust thickness change that is bounded by large fault system. The inner necking breakaway complexes (F1 and F2) separate a largely unchanged crust and the Mesozoic units have a flat bedding. The outer breakaway complex (F3) defines the distal edge of the necking domain, where crust thickness is ~5-10 km. Further southward, crust thickness shows little change.

Inner necking breakaway

The inner necking breakaway consists of two fault segments, F1 and F2 (Fig. 11). F1 can be observed in sections E-E', F-F', and G-G' (Figs. 8-10). The western and eastern parts of F1 is not covered by our seismic data and it is thus hard to define its full extent. F1 has the maximum throw of 2 s (TWT), which decreases to the west. It has a high-angle (45°) geometry in section F-F' that concaves downward to low-angle (~20°) in section G-G'. F2 can be observed in section C-C', D-D', E-E' and F-F' (Figs. 6-9). The maximum fault throw is ~1 s (TWT) in D-D'. Fault displacement variation of F1, which changes from the maximum (2 s, TWT) in G-G' to the minimum in E-E' (~0 s, TWT), and F2, which changes from the maximum (1 s, TWT) in D-D' to the minimum (0 s, TWT), across the studied area suggests that these fault segments may have kinematically linked during rifting. They form as an en-echelon fault array that controlled the deformations of the inner necking domain.

Outer necking breakaway

The outer necking breakaway consists of a complex low-angle fault system that is dominated by fault splays (Fig. 11). This fault system can be observed in all seismic sections from A-A' to G-G'. The number of faults changes laterally from one in sections A-A' and B-B' to two in sections C-C', E-E', and G-G', to four in section D-D', and to three in section E-E' (Fig. 11). The complex fault splay architecture may indicate that the outer necking breakaway consists of a nest of interactive fault network. The maximum fault displacement is located in the central part of the necking zone, which show fault throw of ~2 s (TWT) and fault heave of <5 km. The development of outer necking breakaway is linked to significant continental crust thinning to ~5 km. It removed the upper homogeneous basement and exhumed the layered lower crust. In the footwall of this fault complex, seismic Moho flattens toward the distal domain in the south (Fig. 3d).

Accepted manuscript

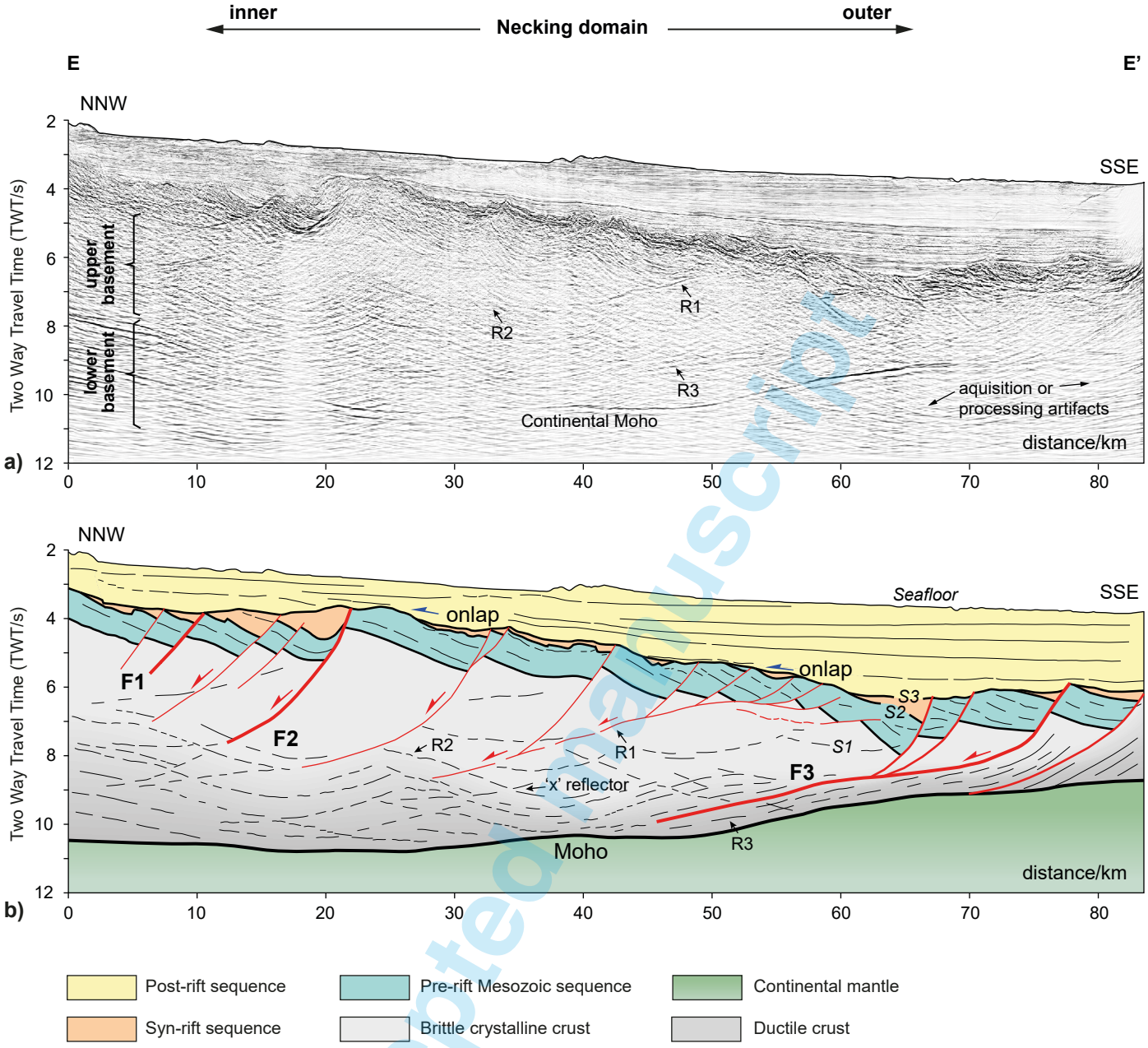

Fig. 8 - Uninterpreted seismic section E-E' (a) and its interpretation (b) showing detailed deformation of the necking domain (section location in Fig. 2). F1 is the inner breakaway complex and F3 is the outer breakaway complex. Note that F1 dips at ~45° and F3 dips at <15°. F3 consists of three splay faults that detach along the layered lower crust. S1, S2, and S3 are three unconformities that separate the top-basement, pre-rift, syn-rift, and post-rift sequences. R1, R2, and R3 are three types of reflectors in the basement.

Accepted manuscript

DISCUSSION

Basin deposition and crustal flexing

Basin deposition of the necking zone in the northeastern South China Sea includes pre-, syn- and post-rift strata. The pre-rift sedimentary rocks are residual of Mesozoic basin stratigraphy (Shi & Li, 2012; Liao et al., 2016; Lin et al., 2021). The syn-rift strata are less then 2 km in thickness and are predominantly restricted in half-grabens. This observation is compatible with regional setting in the early Cenozoic (37-58 Ma), during which discrete rift faults were widely distributed in a broad area (>200-km-wide rift belt) of the South China Sea (Lin et al., 2003; Huang et al., 2012). This is, however, different from our observations in the necking domain of the northeastern South China Sea, where the dip of faults and fractures change progressively from high-angle (~45°) in the inner necking domain to low-angles (<10°). Therefore, the deposition of syn-rift strata in the distal part of the necking domain may have been partly controlled by low-angle faults. The post-rift strata have the maximum thickness along the axis of the "failed rift" (Fig. 3d). It shows landward migration of stratigraphic onlaps over S2.

One of the important observations in the necking domain is the downward tilting (~10°) of continental crust. Crustal block tilting could be a response to many processes, including (1) post-rift sediment loading (Clift et al., 2002, 2015; Morley & Westaway, 2006; Clift, 2015), (2) post-rift thermal subsidence (White & McKenzie, 1988), (3) fault bounded block rotation

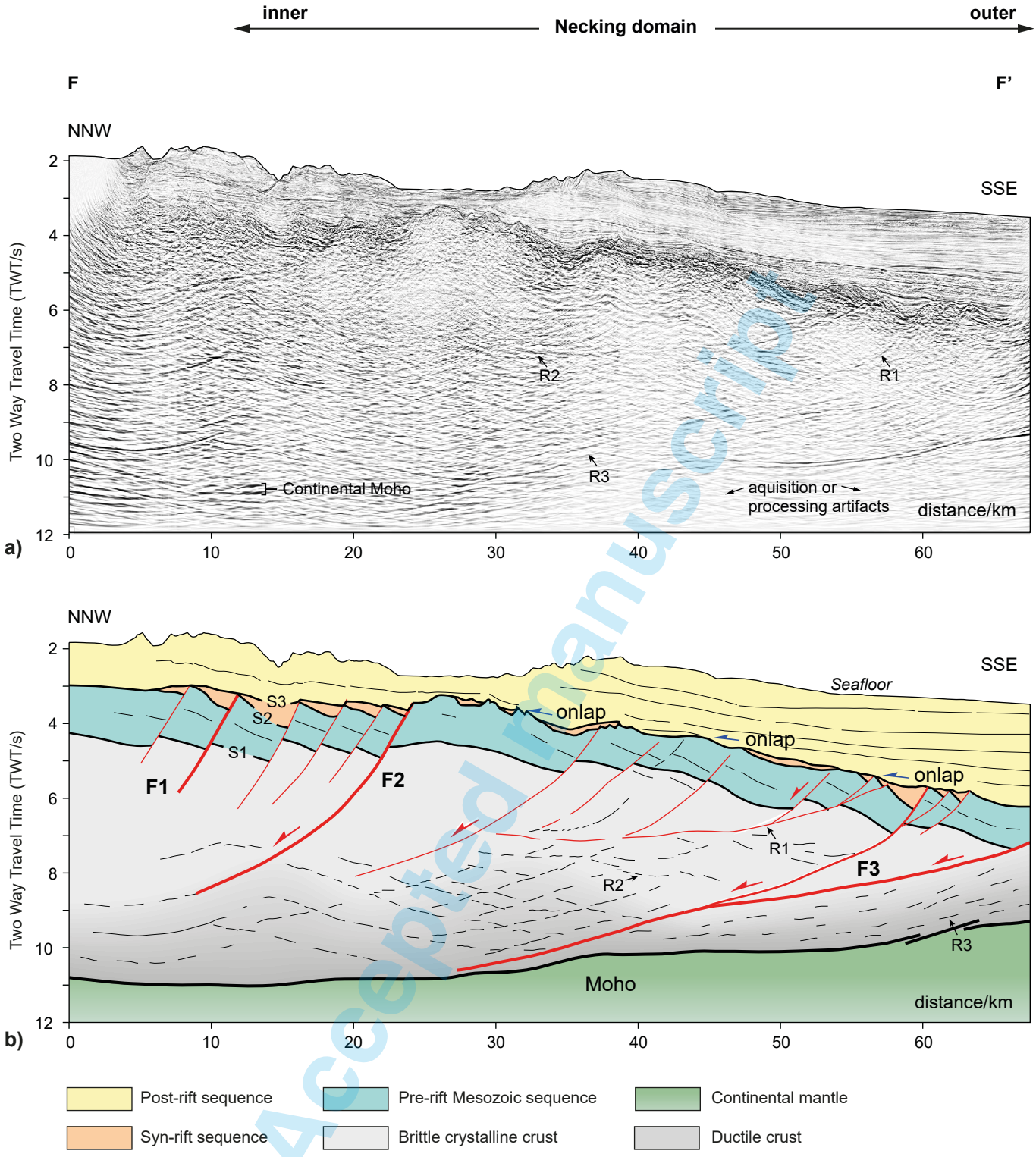

Accepted manuscript

Fig. 9 - Uninterpreted seismic section F-F' (a) and its interpretation (b) showing detailed deformation of the necking domain (section location in Fig. 2). F1 is the inner breakaway complex and F3 is the outer breakaway complex. F1 dips at ~45° and F3 dips at 10-15°. S1, S2, and S3 are three unconformities that separate the top-basement, pre-rift, syn-rift, and post-rift sequences. R1, R2, and R3 are three types of reflectors in the basement. Note that crustal thickness shows few changes in the hangingwall of F1.

(Wernicke & Burchfiel, 1982), and (4) syn-rift crustal flexure (Geoffroy et al., 1998, 2015; Geoffroy, 2005). In our case, the seismic characteristics within the post-rift succession show a "steer-head" geometry (Fig. 2c, White & McKenzie, 1988) with opposite-dipping seismic reflection, symmetrical around the rift axis (Fig. 2d). This indicates that the contribution of post-rift loading and thermal subsidence played an important role in the downward flex of the northeastern continental margin (Fig. 11). Fault bounded block rotation in the northeastern South China Sea is limited, as the outer necking breakaway only show <5 km of displacement. However, the tilting of the necking domain may not be entirely controlled by thermal subsidence and sediments

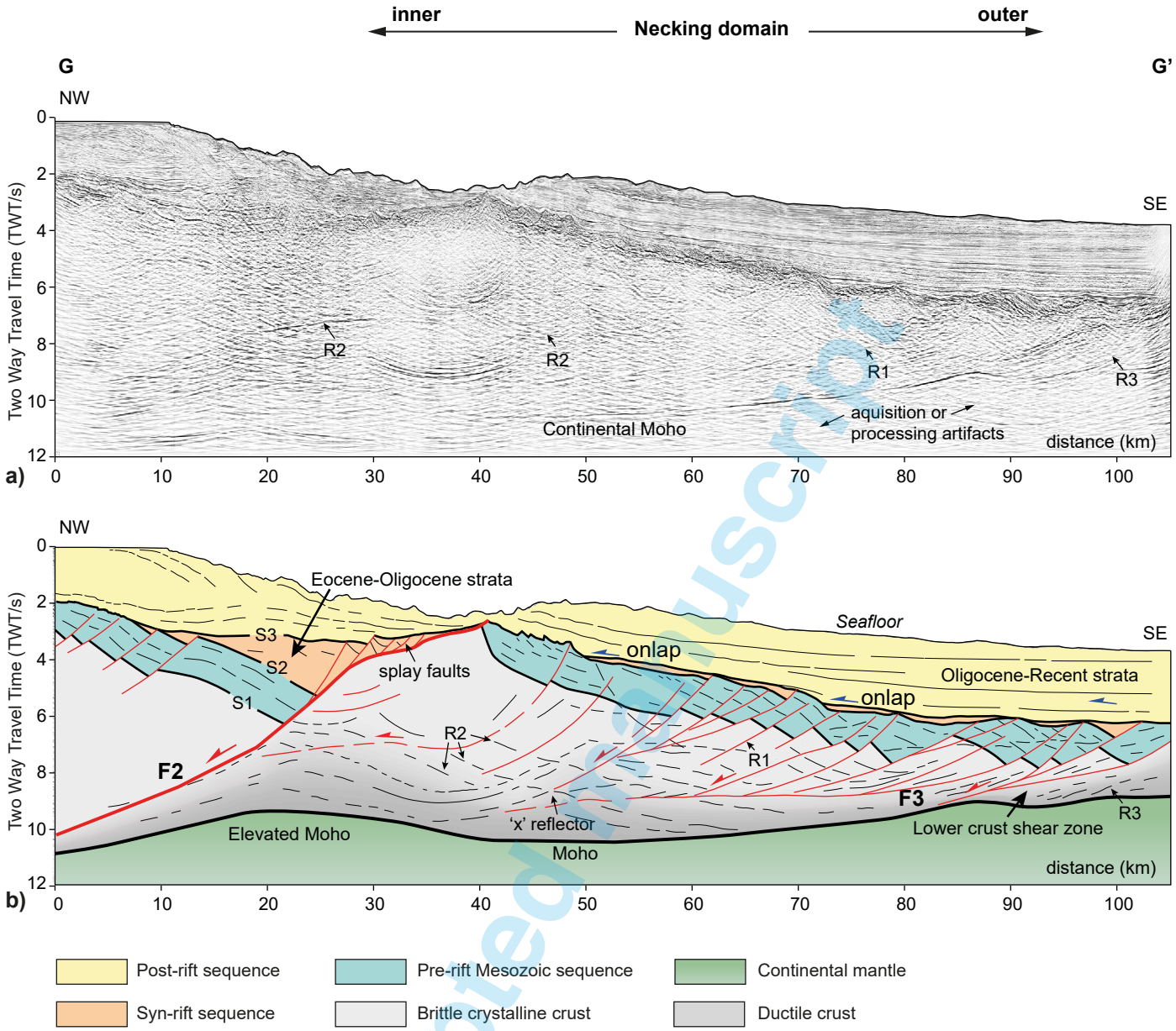

Fig. 10 - Uninterpreted seismic section G-G' (a) and its interpretation (b) showing detailed deformation of the necking domain (section location in Fig. 2). F2 is the inner breakaway complex and F3 is the outer breakaway complex. Note that F2 changes its dip from high angle (~40°) in the lower sector to low angle (~15°) in the upper sector. Several small splay faults are observed in the hangingwall. In the central part of the necking domain, the tilted fault block is highly-faulted by large numbers of small-scaled faults. F3 consists of four splay faults. S1, S2, and S3 are three unconformities that separate the top-basement, pre-rift, syn-rift, and post-rift sequences. R1, R2, and R3 are three types of reflectors in the basement.

loading. We can see that the Mesozoic strata gradually tilt towards the rift axis, forming a flexure (Figs. 5-6 and 8-9).

Crustal flexing has been recorded in many extended areas, such as the east and west Greenland (Geoffroy et al., 1998; Skaarup & Pulvertaft, 2007), Lebombo monocline in Mozambique (Klausen, 2009), and Afar rift (Le Gall et al., 2011; Corti et al., 2015; Stab et al., 2016). The flexing of continental necking domain has been recognized as an important characteristic of volcanic margins (Geoffroy, 2005; Corti et al., 2015). The formation of flexure zone has been explained as a rollover anticline developed above a continentward-dipping detachment based on outcrop studies of east Greenland margin (Geoffroy et al., 1998), although deep structures of the proposed detachment fault have not been clearly resolved in seismic data (Chalmers et al., 1999). Corti et al. (2015) suggests that the flexing of continental necking zone is caused by flexural loading due to magmatic intrusions. Analogue modeling by Zwaan et al. (2020) suggests that differential extension of a weak lower crust, potentially enhanced by magmatic additions, can plausibly explain margin flexure. However, the modelling results show faults that are dominated by seaward-dipping rather than landward-dipping faults, different from observations in field exposures and submarine data (Geoffroy et al., 1998; Stab et al., 2016). In our study, the downward tilting and flexing of continental crust at the necking domain may have been partly controlled by the thinning of the lower basement, as it is observed in Figure 11 where all the seismic sections show

Accepted manuscript

a rapid thinning of layered reflection towards the outer domain. This observation is concordant with limited fault control on the formation of necking flex.

ILndward dipping structures

The most striking characteristic of the bended or flexed necking domain in the northeastern South China Sea is the densely-spaced, landward-dipping faults and fractures that are organized in a domino configuration in the homogeneous basement (Fig. 11). These observations suggest that the homogeneous basement may be dominated by brittle deformations (Fig. 12, faults and fractures). A similar reflection pattern has been observed and identified in many other rifted margins (e.g., Phillips et al., 2016; Deng and McClay, 2019, 2021; Gresseth et al., 2021). These crustal scale structures sole into the lower crust, showing progressive dip change from 45° in the inner necking zone to <10° in the outer necking zone. This type of persistent deformation across the necking domain may suggest top-to-the-continent sense of crust movement with respect to the mantle during crustal necking. Similar observations have been identified in the Afar Depression and the Main Ethiopian Rift in East Africa (Le Gall et al., 2011; Corti et al., 2015; Stab et al., 2016) and East Greenland (Geoffroy et al., 1998; Lenoir et al., 2003). Recent studies of rifted margins have also revealed that the development of predominantly landward-dipping faults in magma-rich passive margins (Geoffroy, 2005; Geoffroy et al., 2015, 2020; Guan et al., 2019) and magma-poor passive margins was associated with strong ductile deformation (Clerc et al., 2015, 2018).

Clerc et al. (2018) suggests that the development of landward dipping faults could be the result of (1) fault inversion, (2) basal shear induced by lithosphere-asthenosphere uprising, (3) gravity collapse caused by plume uprising. Corti et al. (2015) proposed that magmatic intrusion could thermally weaken crust strength and result in significant downward flexing. Zwaan et al. (2020) explained that differential extension of a weak crust aided by magmatic loading could result in crustal-scale marginal flexure.

Accepted manuscript

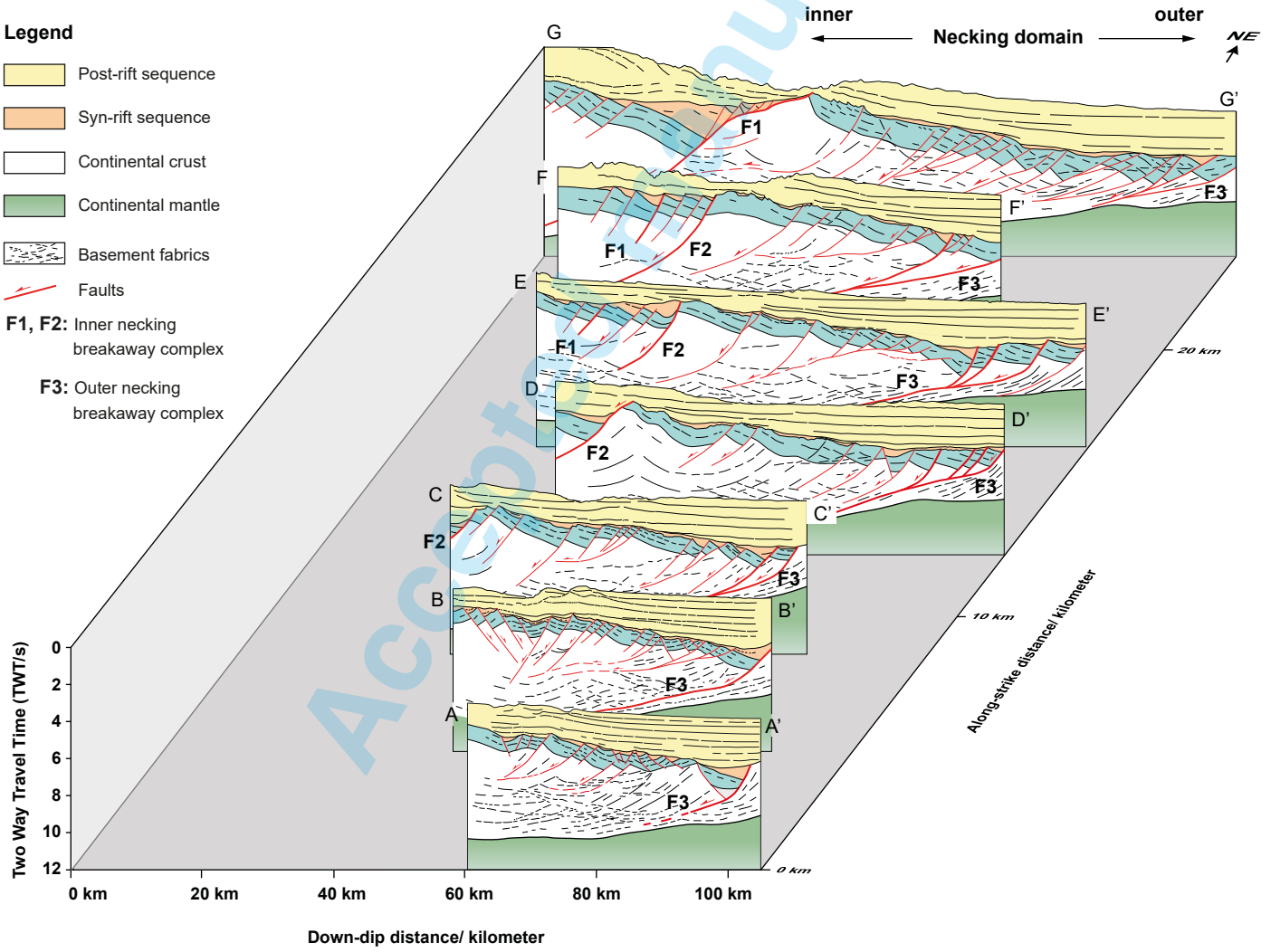

Fig. 11 - Isometric sections (A-A' to G-G') across the necking domain of the northeastern South China Sea showing the structural architecture of the studied area (seismic lines location in Fig. 2). F1, F2, and F3 are breakaway complexes of the necking domain and F4 is the breakaway complex of the distal domain. The inner breakaway complex consists of two, left-stepping fault segments F1 and F2. The inner breakaway complex, F3, consists of several splay faults. Note that the lateral and down-dip changes of the necking domain is mainly controlled by faults and fractures in the upper part of the crust and by layered reflectors in the lower part of the crust.

In the northeastern South China Sea, our seismic data show no obvious evidence of fault reactivation of inherited contractional faults. Large volumes of magma underplating (as thick as 5 km) have been documented beneath the northern South China Sea margins in forms of high-velocity lower crustal layer (Vp=~7.0–7.6 km/s) (Pin et al., 2001; Wang et al., 2006, 2020; Wan et al., 2017, 2019; Xia et al., 2018; Chiu et al., 2021). In addition, the Moho has been arched upward beneath the central part of the rift basin. The intrusion of magma in the lower crust and upwelling of mantle in the "failed rift" of northeastern South China Sea allow us to infer that weak coupling between the crust and upper mantle may generate top-to-the-continent sense of shear. The shearing is likely further promoted by the movement of layered lower crust that changes its thickness from 6-9 km in the inner necking domain to <3 km in the outer necking domain (Fig. 11). The formation of layered reflections in the lower part of the crust is likely dominated by ductile (mylonitic) shear zone. Similar observations have been reported in many parts of the South China Sea margins (Deng et al., 2020; Xi et al., 2022) and other rifted margins (Allmendinger et al., 1987b; Phillips et al., 2016; Sapin et al., 2021).

Comparison with other margins

Although the Cenozoic rifting of the South China Sea involved widespread magmatism, the margin architecture is different from the typical magma-poor and magma-rich margins (Yeh et al., 2012; Larsen et al., 2018a). In the magma-poor continental margins, such as the fossil Alpine and North Atlantic Iberian-Newfoundland margins, necking domains are suggested to be dominated by decoupled deformation due to the presence of weak, mid-crust layer and brittle upper and lower layers (e.g., Manatschal, 2004; Sutra & Manatschal, 2012; Mohn et al., 2012, 2015; Peron-Pinvidic et al., 2013; Sutra et al., 2013; Haupert et al., 2016; Chenin et al., 2021). Deformation in the necking domain allows significant thinning of the continental crust through the development of detachment faults in the lower and upper crusts that decouples from ductilely deforming middle crust (Mohn et al., 2012). However, this may not be the case in many other extensional regimes and rifted margins that have a different lithospheric strength profile (Huismans and Beaumont, 2011; Peron-Pinvidic and Manatschal, 2019; Sapin et al., 2021). For instance, in the Basin and Range Province of the Western United States and the Aegean of the eastern Mediterranean, which are dominated by weak lower crust and strong upper crust, the crustal necking is dominated by boudinage of upper curst coupled with strong ductile deformation, usually through shear zone in the lower crust (Wernicke, 1992; Jones et al., 1992; Jolivet and Brun, 2010). In fact, many continental margins, such as the South China Sea (Franke et al., 2014; Brune et al., 2017; Deng et al., 2020), South Atlantic margins (Clerc et al., 2018; Epin et al., 2021; Araujo et al., 2022), Gulf of Mexico (Sapin et al., 2021; Izquierdo-

Accepted manuscript

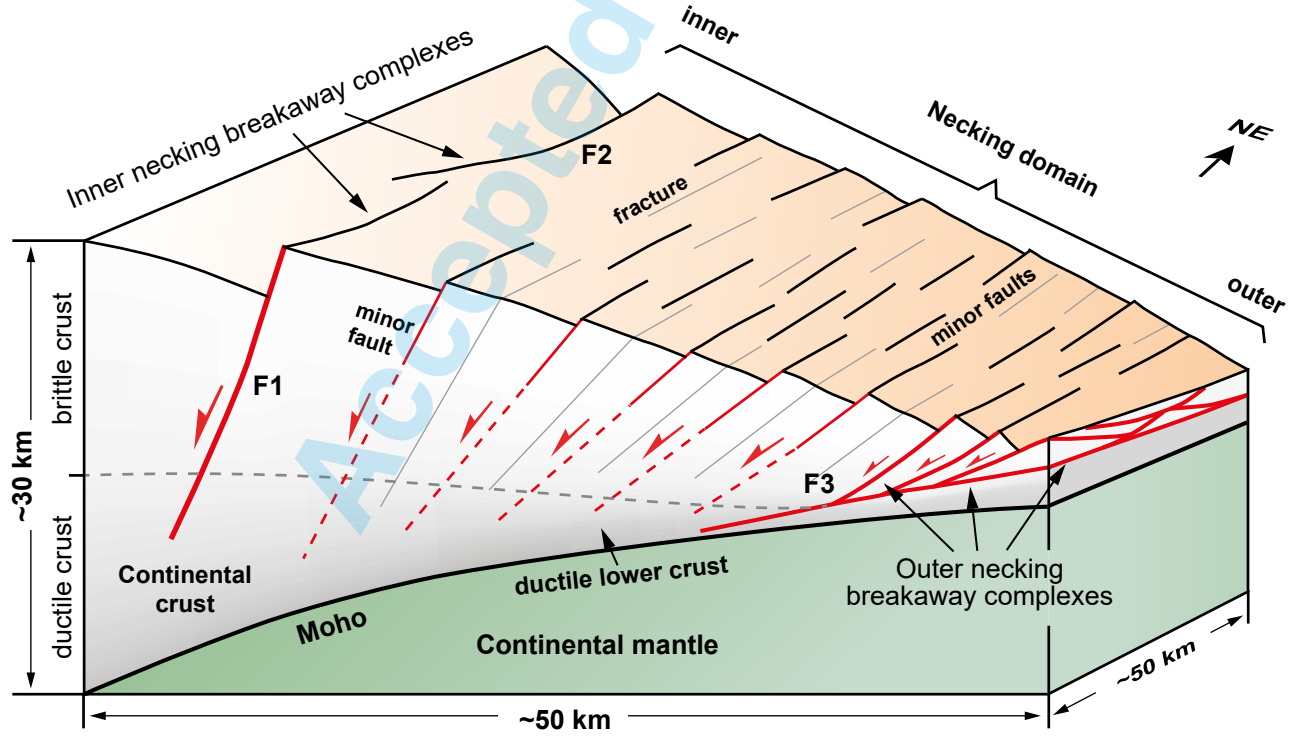

Fig. 12 - Three-dimensional block diagram illustrating the crustal architecture and structures of the necking domain in the northeastern South China Sea. Note that the necking domain has a wedge-shaped geometry tapering to the southeast. The domain-bounding fault systems include inner and outer necking breakaway complexes. The necking domain deformation is dominated by distributed minor faults and fractures in most of the homogeneous crust and localized shear deformation at the bottom of the crust.

Llavall et al., 2022), and Afar rift (Stab et al., 2016; Khalil et al., 2020), show ductile deformations in continental lower crust.

In the northeastern South China Sea, brittle, landward-dipping faults are mainly developed in the homogeneous upper crust that detach into the layered lower crust (Fig. 12). Seismic reflections in the layered lower crust dip at a shallow angle against the seismic Moho, a manifestation of ductile shearing. The southeastward tilting and tapering of the necking domain were facilitated by a weak layer in the lower crust. These observations differ from the crustal deformations in the magma-poor margins as the shear zone, in our case, is located in the layered lower crust, not in the middle crust (e.g., Mohn et al., 2012). The presence of ductile lower crust is likely promoted by high geothermal gradient as a result of strong magmatic intrusion. Magmatic intrusion in the lower crust has been widely recognized by Ocean Bottom Seismic (OBS) data (Lester et al., 2014; Larsen et al., 2018b; Clerc et al., 2018; Sun et al., 2019a; Zhang et al., 2021a; Wen et al., 2021).

Apart from that, the inner and outer breakaway complexes show limited displacement. Most part of the inner breakaway complex dip at ~45° with only the central part of F2 showing fault heave of ~10 km (Fig. 10). The outer breakaway complex has a low-angle geometry (10-15°), but fault displacement along the fault is <10 km (Fig. 11). These observations contrast with the large-magnitude 'breakaway complexes' defined by Osmundsen & Peron-Pinvidic (2018) that commonly have displacement of 20-30 km. We argue that it is likely due to limited seismic data coverage, which only partially image the necking domain. In addition, the observation of large amount of landward-dipping densely-spaced minor faults and fractures of seismic and even subseismic scales, as shown by Gall et al. (2011), indicates that necking deformation may be partitioned by distributed faults in the crust.

Implications for fractured basement reservoir

Our study shows that the necking domain in the northeastern South China Sea is characterized by highly fractured and faulted crystalline basement (Fig. 11). The formation of landward-dipping fractures as a result of top-to-the-continent sense of shear may have yielded fracture networks of seismic and subseismic scales, similar to those observed outcropping in the Afar rift, and the East Greenland (Le Gall et al., 2011; Stab et al., 2016) and East Greenland (Geoffroy et al., 1998; Lenoir et al., 2003). Knowledge of fractured basement provides valuable insights into fault geometries during the development of offshore basins as the fractured basement could form potential reservoirs for hydrocarbon and geothermal resources (Cuong & Warren, 2009; Trice, 2014; Bonter & Trice, 2019; Li et al., 2019; Trice et al., 2019; Banks et al., 2019; Holdsworth et al., 2019; Mado et al., 2020; Xue et al., 2021; Gusti, 2021; You et al., 2021; Dai et al., 2021; Chabani et al., 2021).

In the South China Sea margins, several oil and gas fields have been discovered in highly-fractured basement, including the oil giant of "Bach Ho Field" in the southwestern margin, where a fracture network associated with major structures greatly enhances reservoir permeability (Cuong & Warren, 2009; Kerimov et al., 2019; You et al., 2021). These fractured reservoirs were sourced from Early Cenozoic strata that is dominated by deep lakes and lake bogs. The deposition of these rocks in the early stage of continental rifting forms the main source rock of the South China Sea, which were preserved in half-grabens and were effectively sealed by fine-grained sedimentary rocks of deltas and shelf slope in a post-rift marine environment (Yang et al., 2012; Jiang et al., 2012; Zhao et al., 2021b). Given the source rock and the recharge happens from top to bottom, fractured basement could become a potential reservoir for hydrocarbons and gas flow.

CONCLUSIONS

We use high-resolution, deep seismic across the well-developed necking zone of the northeastern South China Sea to show the crustal architecture and deformations associated with the development of the necking domain. Our observations show first- and second-order deformations of necking zone, which improve our generic understanding of crustal necking deformations worldwide. Our main conclusions are:

1) The necking domain of the northeastern South China Sea has a down-dip width of ~50 km, bounded by inner and outer breakaway complexes. Crustal thinning in the necking zone is dominated by the gradual removal of lower crust towards the outer domain, while the upper crust largely preserves its thickness. In the outer necking domain, the upper crust is bounded by the outer breakaway complex that exhumes the lower crust in its footwall. The necking domain flexes downward and is overlain by distributed syn-rift sequence that is in turn covered by a post-rift sequence, which is up to 6 km thick.
2) The necking domain is characterised by the development of landward-dipping, densely-spaced fractures and faults that show progressive dip change from 45° in the inner necking zone to <10° in the outer necking zone. The change of fault dip is accompanied by a gradual domain rotation from 0° in the inner part to 10° in the outer part. The development of landward dipping, crustal-scale structures suggest top-to-the-continent sense of shear roots over a ductile shear zone in the lower crust.
3) The highly fractured crystalline basement could be the location of ideal reservoirs in the necking domain providing that matured hydrocarbon flow sourced from syn-rift strata was effectively sealed by post-rift fine-grained units. Therefore, the understanding of necking zone deformation could also be helpful for exploration of hydrocarbon and geothermal resources.

ACKNOWLEDGEMENTS

The research is sponsored by National Natural Science Foundation of China No.42272234 and No. 41902123 and China Postdoc Science Foundation No. 2020T130619. The authors thank China National Offshore Oil Corporation (CNOOC) for providing permission to show seismic images from northern South China Sea. Easycopy is thanked for kindly providing the academic license for seismic imaging. Geosoft is thanked for providing the academic license of Oasis Montaj software to Leeds University.

Accepted manuscript

REFERENCES

Allmendinger R.W. (1983) - Cenozoic and Mesozoic structure of the eastern Basin and Range province, Utah, from COCORP seismic reflection data (USA). Geology, 11, 532-536, https://doi.org/10.1130/0091-7613(1983)11<532:CAMSOT>2.0.CO;2.

Allmendinger R.W., Hauge T.A., Hauser E.C., Potter C.J., Klemperer S.L., Nelson K.D., Knuepfer P. & Oliver J. (1987a) - Overview of the COCORP 40°N Transect, western United States: The fabric of an orogenic belt. Geological Society of America Bulletin, 98, 308, https://doi.org/10.1130/0016-7606(1987)98<308:OOTCNT>2.0.CO;2.

Allmendinger R.W., Nelson K.D., Potter C.J., Barazangi M., Brown L.D. & Oliver J.E. (1987b) - Deep seismic reflection characteristics of the continental crust. Geology, 15, 304, https://doi.org/10.1130/0091-7613(1987)15<304:DSRCOT>2.0.CO;2.

Araujo M.N., Perez-Gussinye M. & Mushaldev I. (2022) - Oceanward rift migration during formation of Santos-Benguela ultra-wide rifted margin: The Geological Society Special Publications, SP524-2021-123, https://doi.org/10.1144/sp524-2021-123.

Bai Y., Dong D., Brune S., Wu S. & Wang Z. (2019) - Crustal stretching style variations in the northern margin of the South China Sea: Tectonophysics, 751, 1-12, https://doi.org/10.1016/j.tecto.2018.12.012.

Banks G., Bernstein S., Salehi S., Guarnieri P., Bird D., Hamblett C., Peacock D. & Foster J. (2019) - Liverpool Land Basement High, Greenland: visualising inputs for fractured crystalline basement reservoir models. Geological Survey of Denmark and Greenland Bulletin, 43, 1-6, https://doi.org/10.34194/GEUSB-201943-02-04.

Barazangi M. & Brown L. (1986) - Reflection seismology: the continental crust, in Barazangi, M. and Brown, L. eds., Geodynamics Series volume 14, Washington, DC, American Geophysical Union, p. 107–119, https://doi.org/10.1002/9781118670118.fmatter.

Bonter D.A. & Trice R. (2019) - An integrated approach for fractured basement characterization: The lancaster field, a case study in the UK. Petroleum Geoscience, 25, 400-414, https://doi.org/10.1144/petgeo2018-152.

Braun J. & Beaumont C. (1989) - A physical explanation of the relation between flank uplifts and the breakup unconformity at rifted continental margins. Geology, 17, 760-764.

Brune S., Heine C., Clift P.D. & Pérez-Gussinyé M. (2017) - Rifted margin architecture and crustal rheology: Reviewing Iberia-Newfoundland, Central South Atlantic, and South China Sea. Marine and Petroleum Geology, 79, 257-281, https://doi.org/10.1016/j.marpetgeo.2016.10.018.

Cai G., Wan Z., Yao Y., Zhong L., Zheng H., Kapsiotis A. & Zhang C. (2019) - Mesozoic northward subduction along the se asian continental margin inferred from magmatic records in the South China sea. Minerals, 9, 598, https://doi.org/10.3390/min9100598.

Callot J.P., Geoffroy L. & Brun J.P. (2002) - Development of volcanic passive margins: Three-dimensional laboratory models: Tectonics, 21, 2-1-2-13, https://doi.org/10.1029/2001TC901019.

Cameselle A.L., Ranero C.R. & Barckhausen U. (2020) - Understanding the 3D Formation of a Wide Rift: The Central South China Sea Rift System: Tectonics, 39, https://doi.org/10.1029/2019tc006040.

Cawood A.J., Ferrill D.A., Morris A.P., Norris D., McCallum D., Gillis E. & Smart K.J. (2021) - Tectonostratigraphic evolution of the Orphan Basin and Flemish Pass region – part 1: results from coupled kinematic restoration and crustal area balancing. Marine and Petroleum Geology, 128, 105042, https://doi.org/10.1016/j.marpetgeo.2021.105042.

Chabani A., Trullenque G., Klee J. & Ledésert B.A. (2021) - Fracture Spacing Variability and the Distribution of Fracture Patterns in Granitic Geothermal Reservoir: A Case Study in the Noble Hills Range (Death Valley, CA, USA): Geosciences, 11, 520, https://doi.org/10.3390/geosciences11120520.

Chalmers J.A., Skaarup N., Pulvertaft T.C.R., Whittaker R.C., Geoffroy L., Skuce A.G., Angelier J., Lepvrier C., GéLard J.P. & Olivier P. (1999) - Discussion on the coastal flexure of Disko (West Greenland), onshore expression of the "oblique reflectors". Journal of the Geological Society, 156, 1051-1055, https://doi.org/10.1144/gsjgs.156.5.1051.

Chang S., Pubellier M., Delescluse M., Qiu Y., Nirrengarten M., Mohn G., Chamot-rooke N. & Liang Y. (2022) - Crustal architecture and evolution of the southwestern South China Sea: Implications to continental breakup. Marine and Petroleum Geology, 136, 105450, https://doi.org/10.1016/j.marpetgeo.2021.105450.

Chang J.H., Yu H.S., Lee T.Y., Hsu H.H., Liu C.S. & Tsai Y.T. (2012) - Characteristics of the outer rise seaward of the Manila Trench and implications in Taiwan-Luzon convergent belt, South China Sea. Marine Geophysical Research, 33, 351-367, https://doi.org/10.1007/s11001-013-9168-6.

Chao P., Manatschal G., Chenin P., Ren J., Zhang C., Pang X., Zheng J., Yang L. & Kusznir N. (2021) - The tectono-stratigraphic and magmatic evolution of conjugate rifted margins: insights from the NW South China Sea. Journal of Geodynamics, 101877, https://doi.org/10.1016/j.jog.2021.101877.

Chauvet F., Sapin F., Geoffroy L., Ringenbach J.-C. & Ferry J.-N. (2021) - Conjugate volcanic passive margins in the austral segment of the South Atlantic – Architecture and development. Earth-Science Reviews, 212, 103461, https://doi.org/10.1016/j.earscirev.2020.103461.

Cheng J., Zhang J., Zhao M., Du F., Wang X. & Qiu X. (2021) - Spatial distribution and origin of the high-velocity lower crust in the northeastern South China Sea. Tectonophysics, 229086, https://doi.org/10.1016/j.tecto.2021.229086.

Chenin P. & Beaumont C. (2013), Influence of offset weak zones on the development of rift basins: Activation and abandonment during continental extension and breakup. Journal of Geophysical Research: Solid Earth, 118, 1698-1720, https://doi.org/10.1002/jgrb.50138.

Chenin P., Manatschal G., Ghienne J. & Chao P. (2021) - The syn-rift tectono-stratigraphic record of rifted margins (Part II): A new model to break through the proximal/distal interpretation frontier. Basin Research, 1-44, https://doi.org/10.1111/bre.12628.

Chenin P., Manatschal G., Picazo S., Müntener O., Karner G., Johnson C. & Ulrich M. (2017) - Influence of the architecture of magma-poor hyperextended rifted margins on orogens produced by the closure of narrow versus wide oceans. Geosphere, 13, GES01363.1, https://doi.org/10.1130/GES01363.1.

Chenin P., Schmalholz S.M., Manatschal G. & Duretz T. (2020) - Impact of crust–mantle mechanical coupling on the topographic and thermal evolutions during the necking phase of 'magma-poor' and 'sediment-starved' rift systems: A numerical modeling study. Tectonophysics, 786, 228472, https://doi.org/10.1016/j.tecto.2020.228472.

Chenin P., Schmalholz S.M., Manatschal G. & Karner G.D. (2018) - Necking of the Lithosphere: A Reappraisal of Basic Concepts With Thermo-Mechanical Numerical Modeling: Journal of Geophysical Research. Solid Earth, 123, 5279-5299, https://doi.org/10.1029/2017JB014155.

Accepted manuscript

Chian D., Louden K.E., Minshull T.A. & Whitmarsh R.B. (1999) - Deep structure of the ocean-continent transition in the southern Iberia Abyssal Plain from seismic refraction profiles: Ocean Drilling Program (Legs 149 and 173) transect. Journal of Geophysical Research: Solid Earth, 104, 7443-7462, https://doi.org/10.1029/1999JB900004.

Chiu H., Wang T.K. & Cho Y.H. (2021) - Crustal underplating and overriding across the collision-subduction transition in the northern Manila subduction zone offshore southwestern Taiwan. Marine Geophysical Research, 42, 22, https://doi.org/10.1007/s11001-021-09444-y.

Clerc C., Jolivet L. & Ringenbach J. (2015) - Ductile extensional shear zones in the lower crust of a passive margin: Earth and Planetary Science Letters, 431, 1-7, https://doi.org/10.1016/j.epsl.2015.08.038.

Clerc C., Ringenbach J.-C., Jolivet L. & Ballard J.-F. (2018) - Rifted margins: Ductile deformation, boudinage, continentward-dipping normal faults and the role of the weak lower crust: Gondwana Research, 53, 20-40, https://doi.org/10.1016/j.gr.2017.04.030.

Clift P.D. (2015) - Coupled onshore erosion and offshore sediment loading as causes of lower crust flow on the margins of South China Sea. Geoscience Letters, 2, 13, https://doi.org/10.1186/s40562-015-0029-9.

Clift P.D., Brune S. & Quinteros J. (2015) - Climate changes control offshore crustal structure at South China Sea continental margin. Earth and Planetary Science Letters, 420, 66-72, https://doi.org/10.1016/j.epsl.2015.03.032.

Clift P., Lin J. & Barckhausen U. (2002) - Evidence of low flexural rigidity and low viscosity lower continental crust during continental break-up in the South China Sea. Marine and Petroleum Geology, 19, 951-970, https://doi.org/10.1016/S0264-8172(02)00108-3.

Corti G., Agostini A., Keir D., Van Wijk J., Bastow I.D. & Ranalli G. (2015) - Magma-induced axial subsidence during final-stage rifting: Implications for the development of seaward-dipping reflectors. Geosphere, 11, 563-571, https://doi.org/10.1130/GES01076.1.

Cui Y., Shao L., Li Z., Zhu W., Qiao P. & Zhang X. (2021) - A Mesozoic Andean-type active continental margin along coastal South China: New geological records from the basement of the northern South. Gondwana Research, 99, 36-52, https://doi.org/10.1016/j.gr.2021.06.021.

Cuong T.X. & Warren J.K. (2009) - Bach ho field, a fractured granitic basement reservoir, Cuu Long Basin, offshore SE Vietnam: A "buried-hill" play. Journal of Petroleum Geology, 32, 129-156, https://doi.org/10.1111/j.1747-5457.2009.00440.x.

Dai X., Tang H., Li H., Zhang Y., Xu P., Wang P., Song G. & Du X. (2021) - Characteristics and formation mechanism of the fractures in Archaean buried hill: A case study in the <scp>BZ19</scp> -6 Block, Bohai Bay Basin, China. Geological Journal, 56, 2240-2257, https://doi.org/10.1002/gj.4052.

Deng H. & McClay K. (2019) - Development of extensional fault and fold system: Insights from 3D seismic interpretation of the Enderby Terrace, NW Shelf of Australia. Marine and Petroleum Geology, 104, 11-28, https://doi.org/10.1016/j.marpetgeo.2019.03.003.

Deng H. & McClay K. (2021) - Three-dimensional geometry and growth of a basement-involved fault network developed during multiphase extension, Enderby Terrace, North West Shelf of Australia. GSA Bulletin, 133, 2051-2078, https://doi.org/10.1130/B35779.1.

Deng H., McClay K. & Belgarde C. (2022) - Low-Angle Normal Faults on the NW Shelf of Australia: Implications for Late Paleozoic Rifting. Tectonics, 41, https://doi.org/10.1029/2021TC007088.

Deng H., Ren J., Pang X., Rey P.F., McClay K.R., Watkinson I.M., Zheng J. & Luo P. (2020) - South China Sea documents the transition from wide continental rift to continental break up. Nature Communications, 11, 4583, https://doi.org/10.1038/s41467-020-18448-y.

Ding W., Sun Z., Mohn G., Nirrengarten M., Tugend J., Manatschal G. & Li J. (2020) - Lateral evolution of the rift-to-drift transition in the South China Sea: Evidence from multi-channel seismic data and IODP Expeditions 367&368 drilling results. Earth and Planetary Science Letters, 531, https://doi.org/10.1016/j.epsl.2019.115932.

Dong S., Gao R., Yin A., Guo T., Zhang Y., Hu J., Li J., Shi W. & Li Q. (2013) - What drove continued continent-continent convergence after ocean closure? Insights from high-resolution seismic-reflection profiling across the Daba Shan in central China. Geology, 41, 671.674, https://doi.org/10.1130/G34161.1.

Eakin D.H., McIntosh K.D., Van Avendonk H.J.A. & Lavier L. (2015) - New geophysical constraints on a failed subduction initiation: The structure and potential evolution of the Gagua Ridge and Huatung Basin. Geochemistry, Geophysics, Geosystems, 16, 380-400, https://doi.org/10.1002/2014GC005548.

Eakin D.H., McIntosh K.D., Van Avendonk H.J.A., Lavier L., Lester R., Liu C.S. & Lee C.S. (2014) - Crustal-scale seismic profiles across the Manila subduction zone: The transition from intraoceanic subduction to incipient collision. Journal of Geophysical Research: Solid Earth, 119, 1-17, https://doi.org/10.1002/2013JB010395.

Epin M.-E., Manatschal G., Sapin F. & Rowan M.G. (2021) - The tectono-magmatic and subsidence evolution during lithospheric breakup in a salt-rich rifted margin: insights from a 3D seismic survey from southern Gabon. Marine and Petroleum Geology, 105005, https://doi.org/10.1016/j.marpetgeo.2021.105005.

Fan C., Xia S., Cao J., Zhao F. & Wan K. (2022) - Seismic constraints on a remnant Mesozoic forearc basin in the northeastern South China Sea. Gondwana Research, 102, 77-94, https://doi.org/10.1016/j.gr.2020.10.006.

Fang P., Ding W., Zhao Y., Lin X. & Zhao Z. (2022) - Detachment-controlled subsidence pattern at hyper-extended passive margin: Insights from backstripping modelling of the Baiyun Rift, northern South China Sea. Gondwana Research, https://doi.org/10.1016/j.gr.2021.12.012.

Franke D. (2013) - Rifting, lithosphere breakup and volcanism: Comparison of magma-poor and volcanic rifted margins. Marine and Petroleum Geology, 43, 63-87.

Franke D., Savva D., Pubellier M., Steuer S., Mouly B., Auxietre J.-L., Meresse F. & Chamot-Rooke N. (2014) - The final rifting evolution in the South China Sea. Marine and Petroleum Geology, 58, 704-720, https://doi.org/10.1016/j.marpetgeo.2013.11.020.

Le Gall B., Daoud M.A., Rolet J. & Egueh N.M. (2011) - Large-scale flexuring and antithetic extensional faulting along a nascent plate boundary in the SE Afar rift. Terra Nova, 23, 416-420, https://doi.org/10.1111/j.1365-3121.2011.01029.x.

Gao J., Peng X., Wu S., Lüdmann T., McIntosh K., Ma B. & Xu Z. (2019) - Different expressions of the crustal structure across the Dongsha Rise along the northeastern margin of the South China Sea: Journal of Asian Earth Sciences, 171, 187-200, https://doi.org/10.1016/j.jseaes.2018.01.034.

Gao J., Wu S., McIntosh K., Mi L., Liu Z. & Spence G. (2016) - Crustal structure and extension mode in the northwestern margin of the South China Sea. Geochemistry, Geophysics, Geosystems, 17, 2143-2167, https://doi.org/10.1002/2016GC006247.

Accepted manuscript

Gao J., Wu S., McIntosh K., Mi L., Yao B., Chen Z. & Jia L. (2015) - The continent-ocean transition at the mid-northern margin of the South China Sea. Tectonophysics, 654, 1-19, https://doi.org/10.1016/j.tecto.2015.03.003.

Geoffroy L., (2005) - Volcanic passive margins. Comptes Rendus Geoscience, 337, 1395-1408, https://doi.org/10.1016/j.crte.2005.10.006.

Geoffroy L., Burov E.B. & Werner P. (2015) - Volcanic passive margins: another way to break up continents: Scientific Reports, 5, 14828, https://doi.org/10.1038/srep14828.

Geoffroy L., Gelard J.P., Lepvrier C. & Olivier P. (1998) - The coastal flexure of Disko (West Greenland), onshore expression of the 'oblique reflectors'. Journal of the Geological Society, 155, 463-473, https://doi.org/10.1144/gsjgs.155.3.0463.

Geoffroy L., Guan H., Gernigon L., Foulger G.R. & Werner P. (2020) - The extent of continental material in oceans: C-Blocks and the Laxmi Basin example. Geophysical Journal International, 222, 1471-1479, https://doi.org/10.1093/gji/ggaa215.

Gouiza M. & Naliboff J. (2021) - Rheological inheritance controls the formation of segmented rifted margins in cratonic lithosphere. Nature Communications, 12, 1-10, https://doi.org/10.1038/s41467-021-24945-5.

Gresseth J.L.S., Braathen A., Serck C.S., Faleide J.I. & Osmundsen P.T. (2021) - Late Paleozoic Supradetachment Basin Configuration in the southwestern Barents Sea - Intrabasement Seismic Facies of the Fingerdjupet Subbasin. Basin Research, https://doi.org/10.1111/bre.12631.

Guan H., Geoffroy L., Gernigon L., Chauvet F., Grigné C. & Werner P. (2019) - Magmatic ocean-continent transitions. Marine and Petroleum Geology, 104, 438-450, https://doi.org/10.1016/j.marpetgeo.2019.04.003.

Gusti U.K. (2021) - Fractured Basement Reservoirs in South Pattani Basin: Seismic Recognition and Integrated Multi-attributes Analysis. Bulletin of Earth Sciences of Thailand, 12, 48-56, https://ph01.tci-thaijo.org/index.php/bestjournal/article/view/246794.

Haji Hassan M.A., Klitzke P. & Franke D. (2020) - The magma-poor Somalian continental margin: Lower crustal boudinage and mantle exhumation. Marine Geology, 430, 106358, https://doi.org/10.1016/j.margeo.2020.106358.

Hao H., Zhang X., You H. & Wang R. (2009) - Characteristics and hydrocarbon potential of Mesozoic strata in eastern Pearl River Mouth basin, northern South China Sea. Journal of Earth Science, 20, 117-123, https://doi.org/10.1007/s12583-009-0013-4.

Harkin C., Kusznir N., Tugend J., Manatschal G. & McDermott K. (2019) - Evaluating magmatic additions at a magma-poor rifted margin: An East Indian case study. Geophysical Journal International, 25-40, https://doi.org/10.1093/gji/ggz007.

Haupert I., Manatschal G., Decarlis A. & Unternehr P. (2016) - Upper-plate magma-poor rifted margins: Stratigraphic architecture and structural evolution. Marine and Petroleum Geology, 69, 241-261, https://doi.org/10.1016/j.marpetgeo.2015.10.020.

Hennig-Breitfeld J., Tim Breitfeld H., Dinh Quang S., Mai Kim V., Van Long T., Thirlwall M. & Xuan Cuong T. (2021) - Ages and character of igneous rocks of the Da Lat Zone in SE Vietnam and adjacent offshore regions (Cuu Long and Nam Con Son basins). Journal of Asian Earth Sciences, 104878, https://doi.org/10.1016/j.jseaes.2021.104878.

Holdsworth R.E., Trice R., Hardman K., McCaffrey K.J.W., Morton A., Frei D., Dempsey E., Bird A. & Rogers S. (2019) - The nature and age of basement host rocks and fissure fills in the Lancaster field fractured reservoir, West of Shetland. Journal of the Geological Society, jgs2019-142, https://doi.org/10.1144/jgs2019-142.

Hsu S.K., Yeh Y.C., Doo, W. Bin & Tsai C.H. (2004) - New bathymetry and magnetic lineations identifications in the northernmost South China Sea and their tectonic implications. Marine Geophysical Research, 25, 29-44, https://doi.org/10.1007/s11001-005-0731-7.

Huang C.-Y., Wang P., Yu M., You C.-F., Liu C.-S., Zhao X., Shao L., Zhong G. & Yumul G.P. (2019) - Potential role of strike-slip faults in opening up the South China Sea. National Science Review, 6, 891-901, https://doi.org/10.1093/nsr/nwz119.

Huang C.Y., Yen Y., Zhao Q.H. & Lin C.T. (2012) - Cenozoic stratigraphy of Taiwan: Window into rifting, stratigraphy and paleoceanography of South China Sea: Chinese Science Bulletin, 57, 3130-3149, https://doi.org/10.1007/s11434-012-5349-y.

Huang C., Zhou D., Sun Z., Chen C. & Hao H. (2005) - Deep crustal structure of Baiyun Sag, northern South China Sea revealed from deep seismic reflection profile. Chinese Science Bulletin, 50, 1131, https://doi.org/10.1360/04wd0207.

Huismans R. & Beaumont C. (2011), Depth-dependent extension, two-stage breakup and cratonic underplating at rifted margins. Nature, 473, 74-78.

Huismans R.S. & Beaumont C. (2007) - Roles of lithospheric strain softening and heterogeneity in determining the geometry of rifts and continental margins. Geological Society Special Publication, 282, 111-138, https://doi.org/10.1144/SP282.6.

Izquierdo-Llavall E., Ringenbach J.C., Sapin F., Rives T. & Callot J.P. (2022) - Crustal structure and lateral variations in the Gulf of Mexico conjugate margins: From rifting to break-up. Marine and Petroleum Geology, 136, 105484, https://doi.org/10.1016/j.marpetgeo.2021.105484.

Jiang Z., Zhu J., Deng H. & Hou D. (2012) - Petroleum System and Hydrocarbon Accumulation Characteristics in the Wenchang and Enping Formations in the Huizhou Sag, Pearl River Mouth Basin, China. Energy Exploration & Exploitation, 30, 351-371, https://doi.org/10.1260/0144-5987.30.3.351.

Jolivet L. & Brun J.-P. (2010) - Cenozoic geodynamic evolution of the Aegean. International Journal of Earth Sciences, 99, 109-138, https://doi.org/10.1007/s00531-008-0366-4.

Jones C.H., Wernicke B.P., Farmer G.L., Walker J.D., Coleman D.S., Mckenna L.W. & Perry F.V. (1992) - Variations across and along a major continental rift: An interdisciplinary study of the Basin and Range Province, western USA. Tectonophysics, 213, 57-96, https://doi.org/10.1016/0040-1951(92)90252-2.

Karner G.D., Johnson C., Shoffner J., Lawson M., Sullivan M., Sitgreaves J., McHarge J., Stewart J. & Figueredo P. (2021) - Tectono-Magmatic Development of the Santos and Campos Basins, Offshore Brazil, in Memoir 124: The Supergiant Lower Cretaceous Pre-Salt Petroleum Systems of the Santos Basin, Brazil. AAPG, 215-256, https://doi.org/10.1306/13722321MSB.9.1853.

Kerimov V.Y., Leonov M.G., Osipov A. V., Mustaev R.N. & Hai, V.N., (2019), Hydrocarbons in the Basement of the South China Sea (Vietnam) Shelf and Structural–Tectonic Model of their Formation. Geotectonics, 53, 42-59, https://doi.org/10.1134/S0016852119010035.

Khalil H.M., Capitanio F.A., Betts P.G. & Cruden A.R. (2020) - 3-D Analog Modeling Constraints on Rifting in the Afar Region. Tectonics, 39, https://doi.org/10.1029/2020TC006339.

Klausen M.B. (2009) - The Lebombo monocline and associated feeder dyke swarm: Diagnostic of a successful and highly volcanic rifted margin? Tectonophysics, 468, 42-62, https://doi.org/10.1016/j.tecto.2008.10.012.

Accepted manuscript

Larsen H.C. et al. (2018a) - Expedition 367/368 summary, in v. 367, https://doi.org/10.14379/iodp.proc.367368.101.2018.

Larsen H.C. et al. (2018b) - Rapid transition from continental breakup to igneous oceanic crust in the South China Sea. Nature Geoscience, 11, 782-789, https://doi.org/10.1038/s41561-018-0198-1.

Lavier L.L. & Manatschal G. (2006) - A mechanism to thin the continental lithosphere at magma-poor margins. Nature, 440, 324-328, https://doi.org/https://doi.org/10.1038/nature04608.

Lenoir X., Féraud G. & Geoffroy L. (2003) - High-rate flexure of the East Greenland volcanic margin: constraints from 40Ar/39Ar dating of basaltic dykes. Earth and Planetary Science Letters, 214, 515-528, https://doi.org/10.1016/S0012-821X(03)00392-3.

Lester R., Van Avendonk H.J.A., McIntosh K., Lavier L., Liu C.-S., Wang T.K. & Wu F. (2014) - Rifting and magmatism in the northeastern South China Sea from wide-angle tomography and seismic reflection imaging. Journal of Geophysical Research: Solid Earth, 119, 2305-2323, https://doi.org/10.1002/2013JB010639.

Lester R., McIntosh K., Van Avendonk H.J.A., Lavier L., Liu C.S. & Wang T.K. (2013) - Crustal accretion in the Manila trench accretionary wedge at the transition from subduction to mountain-building in Taiwan. Earth and Planetary Science Letters, 375, 430-440, https://doi.org/10.1016/j.epsl.2013.06.007.

Li J., Chen G., Zhang B., Hong L. & Han Q. (2019) - Structure and fracture-cavity identification of epimetamorphic volcanic-sedimentary rock basement reservoir: a case study from central Hailar Basin, China. Arabian Journal of Geosciences, 12, https://doi.org/10.1007/s12517-018-4221-z.

Li Y., Huang H., Grevemeyer I., Qiu X., Zhang H. & Wang Q. (2021) - Crustal structure beneath the Zhongsha Block and the adjacent abyssal basins, South China Sea: New insights into rifting and initiation of seafloor spreading. Gondwana Research, 99, 53-76, https://doi.org/10.1016/j.gr.2021.06.015.

Li Z.X., Li X.H., Chung S.L., Lo C.H., Xu X. & Li W.X. (2012) - Magmatic switch-on and switch-off along the South China continental margin since the Permian: Transition from an Andean-type to a Western Pacific-type plate boundary. Tectonophysics, 532-535, 271-290, https://doi.org/10.1016/j.tecto.2012.02.011.

Li F., Sun Z. & Yang H. (2018) - Possible Spatial Distribution of the Mesozoic Volcanic Arc in the Present-Day South China Sea Continental Margin and Its Tectonic Implications. Journal of Geophysical Research: Solid Earth, 123, 6215-6235, https://doi.org/10.1029/2017JB014861.

Li F., Sun Z., Yang H., Lin J., Stock J.M., Zhao Z., Xu H. & Sun L. (2020) - Continental Interior and Edge Breakup at Convergent Margins Induced by Subduction Direction Reversal: A Numerical Modeling Study Applied to the South China Sea Margin. Tectonics, 39, 1-18, https://doi.org/10.1029/2020TC006409.

Li J., Zhang Y., Dong S. & Johnston S.T. (2014) - Cretaceous tectonic evolution of South China: A preliminary synthesis: Earth-Science Reviews, 134, 98-136, https://doi.org/10.1016/j.earscirev.2014.03.008.

Li C.F., Zhou Z., Hao H., Chen H., Wang J., Chen B. & Wu J. (2008) - Late Mesozoic tectonic structure and evolution along the present-day northeastern South China Sea continental margin. Journal of Asian Earth Sciences, 31, 546-561, https://doi.org/10.1016/j.jseaes.2007.09.004.

Li C.-F., Zhou Z., Li J., Hao H. & Geng J. (2007) - Structures of the northeasternmost South China Sea continental margin and ocean basin: geophysical constraints and tectonic implications. Marine Geophysical Researches, 28, 59-79, https://doi.org/10.1007/s11001-007-9014-9.

Liang, Y. et al. (2019) - Décollements, Detachments, and Rafts in the Extended Crust of Dangerous Ground, South China Sea: The Role of Inherited Contacts. Tectonics, 1863-1883, https://doi.org/10.1029/2018TC005418.

Liao W.Z., Lin A.T., Liu C.S., Oung J.N. & Wang Y. (2016) - A study on tectonic and sedimentary development in the rifted northern continental margin of the South China Sea near Taiwan. Interpretation, 4, SP47-SP65, https://doi.org/10.1190/INT-2015-0209.1.

Lin A.T. & Watts A.B. (2002) - Origin of the West Taiwan basin by orogenic loading and flexure of a rifted continental margin. Journal of Geophysical Research: Solid Earth, 107, ETG 2-1-ETG 2-19, https://doi.org/10.1029/2001jb000669.

Lin A.T., Watts A.B. & Hesselbo S.P. (2003) - Cenozoic stratigraphy and subsidence history of the South China Sea margin in the Taiwan region. Basin Research, 15, 453-478, https://doi.org/10.1046/j.1365-2117.2003.00215.x.

Lin J., Xu Y., Sun Z. & Zhou Z. (2019) - Mantle upwelling beneath the South China Sea and links to surrounding subduction systems. National Science Review, 6, 877-881, https://doi.org/10.1093/nsr/nwz123.

Lin A.T., Yang C.C., Wang M.H. & Wu J.C. (2021) - Oligocene-Miocene sequence stratigraphy in the northern margin of the South China Sea: An example from Taiwan. Journal of Asian Earth Sciences, 213, 104765, https://doi.org/10.1016/j.jseaes.2021.104765.

Liu S., Zhao M., Sibuet J.C., Qiu X., Wu J., Zhang J., Chen C., Xu Y. & Sun L. (2018) - Geophysical constraints on the lithospheric structure in the northeastern South China Sea and its implications for the South China Sea geodynamics. Tectonophysics, 742-743, 101-119, https://doi.org/10.1016/j.tecto.2018.06.002.

Lymer G., Cresswell D.J.F., Reston T.J., Bull J.M., Sawyer D.S., Morgan J.K., Stevenson C., Causer A., Minshull T.A. & Shillington D.J. (2019) - 3D development of detachment faulting during continental breakup. Earth and Planetary Science Letters, 515, 90-99, https://doi.org/10.1016/j.epsl.2019.03.018.

Mado M., Kessler F.L., Jong J. & Am M.K.A. (2020) - "Fractured basement" play in the Sabah Basin? – the Crocker and Kudat formations as hydrocarbon reservoirs and their risk factors. Bulletin of the Geological Society of Malaysia, 69, 157-171, https://doi.org/10.7186/bgsm69202014.

Mai H.A., Chan Y.L., Yeh M.W. & Lee T.Y. (2018) - Tectonic implications of Mesozoic magmatism to initiation of Cenozoic basin development within the passive South China Sea margin. International Journal of Earth Sciences, 107, 1153-1174, https://doi.org/10.1007/s00531-017-1537-y.

Manatschal G. (2004) - New models for evolution of magma-poor rifted margins based on a review of data and concepts from West Iberia and the Alps. International Journal of Earth Sciences, 93, 432-466, https://doi.org/10.1007/s00531-004-0394-7.

Manatschal G., Lavier L. & Chenin P. (2015) - The role of inheritance in structuring hyperextended rift systems: Some considerations based on observations and numerical modelling. Gondwana Research, 27, 140-164, https://doi.org/10.1016/j.gr.2014.08.006.

McClay K. & Hammerstein J. (2020) – Introduction. Geological Society, London, Special Publications, SP476-2019-246, https://doi.org/10.1144/SP476-2019-246.

McDermott K., Gillbard E. & Clarke N. (2015) - From Basalt to Skeletons – the 200 million-year history of the Namibian margin uncovered by new seismic data. First Break, 33, https://doi.org/10.3997/1365-2397.33.12.83748.

Accepted manuscript

McIntosh K., Lavier L., van Avendonk H., Lester R., Eakin D. & Liu C.S. (2014) - Crustal structure and inferred rifting processes in the northeast South China Sea. Marine and Petroleum Geology, 58, 612-626, https://doi.org/10.1016/j.marpetgeo.2014.03.012.

McKenzie D. (1978) - Some remarks on the development of sedimentary basins: Earth and Planetary Science Letters, 40, 25-32.

Minshull T. A., Dean S.M., Whitmarsh R.B., Russell S.M., Louden K.E. & Chian D. (1998) - Deep structure in the vicinity of the ocean-continent transition zone under the southern Iberia Abyssal Plain. Geology, 26, 743, https://doi.org/10.1130/0091-7613(1998)026<0743:DSITVO>2.3.CO;2.

Mjelde R., Raum T., Kandilarov A., Murai Y. & Takanami T. (2009) - Crustal structure and evolution of the outer Møre Margin, NE Atlantic: Tectonophysics, 468, 224-243, https://doi.org/10.1016/j.tecto.2008.06.003.

Mohn G., Karner G., Manatschal G. & Johnson C. (2015) - Structural and stratigraphic evolution of the Iberia and Newfoundland hyper-extended rifted margins: A quantitative modeling approach. Geological Society, London, Special Publications, 16, 9156, https://doi.org/10.1144/SP413.9.

Mohn G., Manatschal G., Beltrando M., Masini E. & Kusznir N. (2012) - Necking of continental crust in magma-poor rifted margins: Evidence from the fossil Alpine Tethys margins. Tectonics, 31, p. n/a-n/a, https://doi.org/10.1029/2011TC002961.

Mohn G., Manatschal G., Müntener O., Beltrando M. & Masini E. (2010) - Unravelling the interaction between tectonic and sedimentary processes during lithospheric thinning in the Alpine Tethys margins. International Journal of Earth Sciences, 99, 75-101, https://doi.org/10.1007/s00531-010-0566-6.

Morley C.K. & Westaway R. (2006) - Subsidence in the super-deep Pattani and Malay basins of Southeast Asia: a coupled model incorporating lower-crustal flow in response to post-rift sediment loading: Basin Research, 18, 51-84, https://doi.org/10.1111/j.1365-2117.2006.00285.x.

Mortimer E.J., Gouiza M., Paton D.A., Stanca R., Rodriguez K., Hodgson N. & Hussein A.A. (2020) - Architecture of a magma poor passive margin – Insights from the Somali margin: Marine Geology, 428, 106269, https://doi.org/10.1016/j.margeo.2020.106269.

Naliboff J.B., Buiter S.J.H., Péron-Pinvidic G., Osmundsen P.T. & Tetreault J. (2017) - Complex fault interaction controls continental rifting. Nature Communications, 8, 1179, https://doi.org/10.1038/s41467-017-00904-x.

Nemčok M. et al. (2022) - Crust first/mantle second and mantle first/crust second; lithospheric breakup scenarios along the Indian margins. Geological Society, London, Special Publications, SP524-2021-109, https://doi.org/10.1144/SP524-2021-109.

Nirrengarten M., Mohn G., Schito A., Corrado S., Gutiérrez-garcía L., Alan S. & Despinois F. (2019) - The thermal imprint of continental breakup during the formation of the South China Sea. Earth and Planetary Science Letters, 1, 115972, https://doi.org/10.1016/j.epsl.2019.115972.

Nissen S.S. (1995) - Deep penetration seismic soundings across the northern margin of the South China Sea. Journal of Geophysical Research, 100, https://doi.org/10.1029/95jb01866.

Nissen S.S., Hayes D.E., Bochu Y., Weijun Z., Yongqin C. & Xiaupin N. (1995) - Gravity, heat flow, and seismic constraints on the processes of crustal extension: northern margin of the South China Sea. Journal of Geophysical Research, 100, https://doi.org/10.1029/95jb01868.

Osmundsen P.T. & Ebbing J. (2008) - Styles of extension offshore mid-Norway and implications for mechanisms of crustal thinning at passive margins. Tectonics, 27, https://doi.org/10.1029/2007TC002242.

Osmundsen P.T. & Péron-Pinvidic G. (2018) - Crustal-Scale Fault Interaction at Rifted Margins and the Formation of Domain-Bounding Breakaway Complexes: Insights From Offshore Norway. Tectonics, 37, 935-964, https://doi.org/10.1002/2017TC004792.

Paton D.A., Pindell J., McDermott K., Bellingham P. & Horn B. (2017) - Evolution of seaward-dipping reflectors at the onset of oceanic crust formation at volcanic passive margins: Insights from the South Atlantic. Geology, 45, 439-442, https://doi.org/10.1130/G38706.1.

Peron-Pinvidic G. & Manatschal G. (2019) - Rifted Margins: State of the Art and Future Challenges. Frontiers in Earth Science, 7, 1-8, https://doi.org/10.3389/feart.2019.00218.

Péron-Pinvidic G. & Manatschal G. (2009) - The final rifting evolution at deep magma-poor passive margins from Iberia-Newfoundland: a new point of view. International Journal of Earth Sciences, 98, 1581-1597, https://doi.org/10.1007/s00531-008-0337-9.

Peron-Pinvidic G., Manatschal G. & Osmundsen P.T. (2013) - Structural comparison of archetypal Atlantic rifted margins: A review of observations and concepts. Marine and Petroleum Geology, 43, 21-47, https://doi.org/10.1016/j.marpetgeo.2013.02.002.

Peron-Pinvidic G. & Naliboff J. (2020) - The exhumation detachment factory: Geology, 48, 635-639, https://doi.org/10.1130/G47174.1.

Peron-Pinvidic G. & Osmundsen P.T. (2016) - Architecture of the distal and outer domains of the mid-Norwegian rifted margin: Insights from the Rån-Gjallar ridges system. Marine and Petroleum Geology, 77, 280-299, https://doi.org/10.1016/j.marpetgeo.2016.06.014.

Peron-Pinvidic G. & Osmundsen P.T. (2018) - The Mid Norwegian - NE Greenland conjugate margins: Rifting evolution, margin segmentation, and breakup. Marine and Petroleum Geology, 98, 162-184, https://doi.org/10.1016/j.marpetgeo.2018.08.011.

Phillips T.B., Jackson C.A.L., Bel R.E., Duffy O.B. & Fossen H. (2016) - Reactivation of intrabasement structures during rifting: A case study from offshore southern Norway. Journal of Structural Geology, 91, 54-73, https://doi.org/10.1016/j.jsg.2016.08.008.

Pin Y., Di Z. & Zhaoshu L. (2001) - A crustal structure profile across the northern continental margin of the South China Sea. Tectonophysics, 338, 1-21, https://doi.org/10.1016/S0040-1951(01)00062-2.

Pindell J., Graham R. & Horn B. (2014) - Rapid outer marginal collapse at the rift to drift transition of passive margin evolution, with a Gulf of Mexico case study. Basin Research, 26, 701-725, https://doi.org/10.1111/bre.12059.

Pindell J. & Heyn T. (2022) - Dynamo-thermal subsidence and sag–salt section deposition as magma-rich rifted margins move off plume centres along incipient lines of break-up. Journal of the Geological Society, 179, jgs2021- 095, https://doi.org/10.1144/jgs2021-095.

Pouliquen G., Connard G., Kearns H., Gouiza M. & Paton D. (2017) - Public domain satellite gravity inversion offshore Somalia combining layered-Earth and voxel based modelling. First Break, 35, https://doi.org/10.3997/1365-2397.35.9.90113.

Le Pourhiet L., Chamot-Rooke N., Delescluse M., May D.A., Watremez L. & Pubellier M. (2018) - Continental break-up of the South China Sea stalled by far-field compression. Nature Geoscience, 11, 605-609, https://doi.org/10.1038/s41561-018-0178-5.

Pubellier M., Aurelio M. & Sautter B. (2018) - The life of a marginal basin depicted in a structural map of the South China Sea. Episodes, 41, 139-142, https://doi.org/10.18814/epiiugs/2018/018014.

Ranero C.R. & Pérez-Gussinyé M. (2010) - Sequential faulting explains the asymmetry and extension discrepancy of conjugate margins. Nature, 468, 294-299, https://doi.org/10.1038/nature09520.

Geological magazine

Reuber K., Mann P. & Pindell J. (2019) - Hotspot origin for asymmetrical conjugate volcanic margins of the austral South Atlantic Ocean as imaged on deeply penetrating seismic reflection lines. Interpretation, 7, SH71–SH97, https://doi.org/10.1190/INT-2018-0256.1.

Ribes C., François J., Gianreto G., Nicolas M., Asta D., Stockli D.F., Galster F., Gillard M. & Karner G.D. (2020) - The Grès Singuliers of the Mont Blanc region (France and Switzerland): stratigraphic response to rifting and crustal necking in the Alpine Tethys. International Journal of Earth Sciences, https://doi.org/10.1007/s00531-020-01902-z.

Sapin F., Ringenbach J.-C. & Clerc C. (2021) - Rifted margins classification and forcing parameters: Scientific Reports, 11, 8199, https://doi.org/10.1038/s41598-021-87648-3.

Savva D., Pubellier M., Franke D., Chamot-Rooke N., Meresse F., Steuer S. & Auxietre J.L. (2014) - Different expressions of rifting on the South China Sea margins: Marine and Petroleum Geology, 58, 579-598, https://doi.org/10.1016/j.marpetgeo.2014.05.023.

Shi H. & Li C.-F. (2012) - Mesozoic and early Cenozoic tectonic convergence-to-rifting transition prior to opening of the South China Sea. International Geology Review, 54, 1801-1828, https://doi.org/10.1080/00206814.2012.677136.

Sibuet J.C., Hsu S.K., Le Pichon X., Le Formal J.P., Reed D., Moore G. & Liu C.S. (2002) - East Asia plate tectonics since 15 Ma: Constraints from the Taiwan region. Tectonophysics, 344, 103-134, https://doi.org/10.1016/S0040-1951(01)00202-5.

Sibuet J.-C., Yeh Y.-C. & Lee C.-S. (2016) - Geodynamics of the South China Sea: Tectonophysics, 692, 98-119, https://doi.org/10.1016/j.tecto.2016.02.022.

Sibuet J.-C., Zhao M., Wu J. & Lee C.-S. (2021) - Geodynamic and plate kinematic context of South China Sea subduction during Okinawa trough opening and Taiwan orogeny. Tectonophysics, 817, 229050, https://doi.org/10.1016/j.tecto.2021.229050.

Sinha S.T., Saha S., Longacre M., Basu S., Jha R. & Mondal T. (2019) - Crustal Architecture and Nature of Continental Breakup Along a Transform Margin: New Insights From Tanzania-Mozambique Margin. Tectonics, 38, 1273-1291, https://doi.org/10.1029/2018TC005221.

Skaarup N. & Pulvertaft T.C.R. (2007) - Aspects of the structure on the coast of the West Greenland volcanic province revealed in seismic data. Bulletin of the Geological Society of Denmark, 55, 65-80, https://doi.org/10.37570/bgsd-2007-55-05.

Stab M., Bellahsen N., Pik R., Quidelleur X., Ayalew D. & Leroy S. (2016) - Modes of rifting in magma-rich settings: Tectono-magmatic evolution of Central Afar. Tectonics, 35, 2-38, https://doi.org/10.1002/2015TC003893.

Stica J.M., Zalán P.V. & Ferrari A.L. (2014) - The evolution of rifting on the volcanic margin of the Pelotas Basin and the contextualization of the Paraná–Etendeka LIP in the separation of Gondwana in the South Atlantic. Marine and Petroleum Geology, 50, 1-21, https://doi.org/10.1016/j.marpetgeo.2013.10.015.

Strachan L.J., Rarity F., Gawthorpe R.L., Wilson P., Sharp I. & Hodgetts D. (2013) - Submarine slope processes in rift-margin basins, Miocene Suez Rift, Egypt. Bulletin of the Geological Society of America, 125, 109-127, https://doi.org/10.1130/B30665.1.

Sun W. (2016) - Initiation and evolution of the South China Sea: an overview. Acta Geochimica, 35, 215-225, https://doi.org/10.1007/s11631-016-0110-x.

Sun Z., Lin J., Qiu N., Jian Z., Wang P., Pang X., Zheng J. & Zhu B. (2019a) - The role of magmatism in the thinning and breakup of the South China Sea continental margin. National Science Review, 6, 871-876, https://doi.org/10.1093/nsr/nwz116.

Sun L., Sun Z., Huang X., Jiang Y. & Stock J.M. (2019b) - Microstructures documenting Cenozoic extension processes in the northern continental margin of the South China Sea. International Geology Review, 00, 1-14, https://doi.org/10.1080/00206814.2019.1669079.

Suo Y., Li S., Jin C., Zhang Y., Zhou J., Li X., Wang P., Liu Z., Wang X. & Somerville I. (2019) - Eastward tectonic migration and transition of the Jurassic-Cretaceous Andean-type continental margin along Southeast China. Earth-Science Reviews, 196, 102884, https://doi.org/10.1016/j.earscirev.2019.102884.

Sutra E. & Manatschal G. (2012) - How does the continental crust thin in a hyperextended rifted margin? Insights from the iberia margin. Geology, 40, 139-142, https://doi.org/10.1130/G32786.1.

Sutra E., Manatschal G., Mohn G. Unternehr P. (2013) - Quantification and restoration of extensional deformation along the Western Iberia and Newfoundland rifted margins. Geochemistry, Geophysics, Geosystems, 14, 2575-2597, https://doi.org/10.1002/ggge.20135.

Theunissen T. & Huismans R.S. (2022) - Mantle exhumation at magma-poor rifted margins controlled by frictional shear zones. Nature Communications, 13, 1634, https://doi.org/10.1038/s41467-022-29058-1.

Trice R. (2014) - Basement exploration, West of Shetlands: progress in opening a new play on the UKCS. Geological Society, London, Special Publications, 397, 81-105, https://doi.org/10.1144/SP397.3.

Trice R., Hiorth C. & Holdswort R. (2019) - Fractured basement play development on the UK and Norwegian rifted margins. Geological Society, London, Special Publications, SP495-18-174, https://doi.org/10.1144/SP495-18-174.

Tsai C.-H., Hsu S.-K., Yeh Y.-C., Lee C.-S. & Xia K. (2004) - Crustal Thinning of the Northern Continental Margin of the South China Sea. Marine Geophysical Researches, 25, 63-78, https://doi.org/10.1007/s11001-005-0733-5.

Tugend J., Gillard M., Manatschal G., Nirrengarten M., Harkin C., Epin M., Saute D., Autin J., Kusznir N. & McDermott K. (2020) - Reappraisal of the magma-rich versus magma-poor rifted margin archetypes. Geological Society, London, Special Publications, 476, 23-47, https://doi.org/10.1144/SP476.9.

Unternehr P., Peron-Pinvidic G., Manatschal G. & Sutra E. (2010) - Hyper-extended crust in the South Atlantic: in search of a model. Petroleum Geoscience, 16, 207-215, https://doi.org/10.1144/1354-079309-904.

Wan X., Li C.F., Zhao M., He E., Liu S., Qiu X., Lu Y. & Chen N. (2019) - Seismic Velocity Structure of the Magnetic Quiet Zone and Continent-Ocean Boundary in the Northeastern South China Sea. Journal of Geophysical Research: Solid Earth, 124, 11866-11899, https://doi.org/10.1029/2019JB017785.

Wan K., Xia S., Cao J., Sun J. & Xu H. (2017) - Deep seismic structure of the northeastern South China Sea: Origin of a high-velocity layer in the lower crust. Journal of Geophysical Research: Solid Earth, 122, 2831-2858, https://doi.org/10.1002/2016JB013481.

Wang T.K., Chen M.K., Lee C.S. & Xia K. (2006) - Seismic imaging of the transitional crust across the northeastern margin of the South China Sea. Tectonophysics, 412, 237-254, https://doi.org/10.1016/j.tecto.2005.10.039.

Wang P., Huang C.-Y., Lin J., Jian Z., Sun Z. & Zhao M. (2019) - The South China Sea is not a mini-Atlantic: plate-edge rifting vs intra-plate rifting. National Science Review, 6, 902-913, https://doi.org/10.1093/nsr/nwz135.

Accepted manuscript

Wang J., Pang X., Liu B., Zheng J. & Wang H. (2018) - The Baiyun and Liwan Sags: Two supradetachment basins on the passive continental margin of the northern South China Sea. Marine and Petroleum Geology, 95, 206-218, https://doi.org/10.1016/j.marpetgeo.2018.05.001.

Wang Q., Zhao M., Zhang H., Zhang J., He E., Yuan Y. & Qiu X. (2020) - Crustal velocity structure of the Northwest Sub-basin of the South China Sea based on seismic data reprocessing. Science China Earth Sciences, 63, 1791-1806, https://doi.org/10.1007/s11430-020-9654-4.

Wen G., Wan K., Xia S., Fan C., Cao J. & Xu H. (2021) - Crustal extension and magmatism along the northeastern margin of the South China Sea: Further insights from shear waves. Tectonophysics, 229073, https://doi.org/10.1016/j.tecto.2021.229073.

Wenker S. & Beaumont C. (2018) - Effects of lateral strength contrasts and inherited heterogeneities on necking and rifting of continents. Tectonophysics, 746, 46-63, https://doi.org/10.1016/j.tecto.2016.10.011.

Wernicke B. (1992) - Cenozoic extensional tectonics of the U.S. Cordillera, in Burchfiel, B.C., Lipman, P.W., and Zoback, M.L. eds., The Cordilleran Orogen, Boulder, Colorado, Geological Society of America, Geology of North America, 553-581, https://doi.org/10.1130/DNAG-GNA-G3.553.

Wernicke B. & Burchfiel B.C. (1982) - Modes of extensional tectonics. Journal of Structural Geology, 4, 105-115.

White N. & McKenzie D. (1988) - Formation of the "'steer's head'" geometry of sedimentary basins by differential stretching of the crust and mantle. Geology, 16, 250-253, https://doi.org/10.1130/0091-7613(1988)016<0250:FOTSSH>2.3.CO;2.

Whitmarsh R.B., Manatschal G. & Minshull T.A. (2001) - Evolution of magma-poor continental margins from rifting to seafloor spreading. Nature, 413, 150-154, https://doi.org/10.1038/35093085.

Wu L., Mei L., Paton D.A., Liu Y., Guo P., Shen C., Liu Z., Luo J., Min C. & Li M. (2020) - Late Cretaceous-Cenozoic intraplate extension and tectonic transitions in eastern China: Implications for intraplate geodynamic origin. Marine and Petroleum Geology, 117, 104379, https://doi.org/10.1016/j.marpetgeo.2020.104379.

Xi P., Li C.-F., Shen C., Liu Y. & Shi H. (2022) - Intra-basement structures and their implications for rifting of the northeastern South China Sea margin. Journal of Asian Earth Sciences, 225, 105073, https://doi.org/10.1016/j.jseaes.2021.105073.

Xia S., Zhao F., Zhao D., Fan C., Wu S., Mi L., Sun J., Cao J. & Wan K. (2018) - Crustal plumbing system of post-rift magmatism in the northern margin of South China Sea: New insights from integrated seismology. Tectonophysics, 744, 227-238, https://doi.org/10.1016/j.tecto.2018.07.002.

Xie X., Ren J., Pang X., Lei C. & Chen H. (2019) - Stratigraphic architectures and associated unconformities of Pearl River Mouth basin during rifting and lithospheric breakup of the South China Sea. Marine Geophysical Research, 40, 129-144, https://doi.org/10.1007/s11001-019-09378-6.

Xu Y., Yan Q., Shi X., Jichao Y., Deng X., Xu W. & Jing C. (2022) - Discovery of Late Mesozoic volcanic seamounts at the ocean-continent transition zone in the Northeastern margin of South China Sea and its tectonic implication. Gondwana Research, https://doi.org/10.1016/j.gr.2022.04.003.

Xue Y., Zhao M. & Liu X. (2021) - Reservoir Characteristics and Controlling Factors of the Metamorphic Buried Hill of Bozhong Sag, Bohai Bay Basin. Journal of Earth Science, 32, 919-926, https://doi.org/10.1007/s12583-021-1415-1.

Yang L., Ren J., McIntosh K., Pang X., Chao L. & Zhao Y. (2018) - The structure and evolution of deepwater basins in the distal margin of the northern South China Sea and their implications for the formation of the continental margin. Marine and Petroleum Geology, 92, 234-254, https://doi.org/10.1016/j.marpetgeo.2018.02.032.

Yang F., Sun Z., Zhou Z., Wu Z., Gao D. & Li Q. (2012) - The Evolution of the South China Sea Basin in the Mesozoic—Cenozoic and Its Significance for Oil and Gas Exploration, in Tectonics and Sedimentation, Tulsa, Oklahoma, American Association of Petroleum Geologists, 397-418, https://doi.org/10.1306/13351562M1003528.

Yeh Y.-C., Hsu S.-K., Doo W.-B., Sibuet J.-C., Liu C.-S. & Lee C.-S. (2012) - Crustal features of the northeastern South China Sea: insights from seismic and magnetic interpretations: Marine Geophysical Research, 33, 307-326, https://doi.org/10.1007/s11001-012-9154-4.

Yeh Y.-C., Sibuet J.-C., Hsu S.-K. & Liu C.-S. (2010) - Tectonic evolution of the Northeastern South China Sea from seismic interpretation. Journal of Geophysical Research, 115, B06103, https://doi.org/10.1029/2009JB006354.

You L., Xu S., Mao X., Zhong J., Jiao Y. & Xiong X. (2021) - Reservoir Characteristics and Genetic Mechanisms of the Mesozoic Granite Buried Hills in the Deep-water of the Qiongdongnan Basin, Northern South China Sea. Acta Geologica Sinica - English Edition, 95, 259-267, https://doi.org/10.1111/1755-6724.14635.

Zhang C. et al. (2021a) - Syn-rift magmatic characteristics and evolution at a sediment-rich margin: Insights from high-resolution seismic data from the South China Sea. Gondwana Research, 91, 81-96, https://doi.org/10.1016/j.gr.2020.11.012.

Zhang Y., Dong S., Wang H., Feng M., Thybo H., Li J., Gao R. & Shi W. (2022) - Coupled Lithospheric Deformation in the Qinling Orogen, Central China: Insights From Seismic Reflection and Surface-Wave Tomography. Geophysical Research Letters, 49, https://doi.org/10.1029/2022GL097760.

Zhang C., Su M., Pang X., Zheng J., Liu B., Sun Z. & Manatschal G. (2019) - Tectono-Sedimentary Analysis of the Hyperextended Liwan Sag Basin (Midnorthern Margin of the South China Sea). Tectonics, 38, 470-491, https://doi.org/10.1029/2018TC005063.

Zhang C., Sun Z., Manatschal G., Pang X., Li S., Sauter D., Péron-Pinvidic G. & Zhao M. (2021b) - Ocean-continent transition architecture and breakup mechanism at the mid-northern South China Sea. Earth-Science Reviews, 103620, https://doi.org/10.1016/j.earscirev.2021.103620.

Zhang Z., Wang L., Liu W., Yan Z., Zhu Y., Zhou S. & Guan S. (2021c) - Mantle serpentinization beneath a failed rift and post-spreading. Geophysical Journal International, https://doi.org/10.1093/gji/ggab006.

Zhao Y., Ding W., Ren J., Li J., Tong D. & Zhang J. (2021a) - Extension Discrepancy of the Hyper-Thinned Continental Crust in the Baiyun Rift, Northern Margin of the South China Sea. Tectonics, https://doi.org/10.1029/2020TC006547.

Zhao M., Qiu X., Xia S., Xu H., Wang P., Wang T.K., Lee C.S. & Xia K. (2010) - Seismic structure in the northeastern South China Sea: S-wave velocity and Vp/Vs ratios derived from three-component OBS data. Tectonophysics, 480, 183-197, https://doi.org/10.1016/j.tecto.2009.10.004.

Zhao Y., Ren J., Pang X., Yang L. & Zheng J. (2018) - Structural style, formation of low angle normal fault and its controls on the evolution of Baiyun Rift, northern margin of the South China Sea: Marine and Petroleum Geology, 89, 687-700, https://doi.org/10.1016/j.marpetgeo.2017.11.001.

Accepted manuscript

Zhao M., Sibuet J.-C. & Wu J. (2019) - Intermingled fates of the South China Sea and Philippine Sea plate: National Science Review, 6, 886-890, https://doi.org/10.1093/nsr/nwz107.

Zhao Z., Zhang H., Cui Y., Tang W. & Qiao P. (2021b) - Cenozoic Sea-land Transition and its Petroleum Geological Significance in the Northern South China Sea. Acta Geologica Sinica - English Edition, 95, 41-54, https://doi.org/10.1111/1755-6724.14628.

Zheng J. & Dai H. (2018) - Subduction and retreating of the western Pacific plate resulted in lithospheric mantle replacement and coupled basin-mountain respond in the North China Craton. Science China Earth Sciences, 61, 406-424, https://doi.org/10.1007/s11430-017-9166-8.

Zhou Y., Liu H., Liu Q., Yan Y., Li Y., Yao Y., Li Y., Liu W. & Zhu R. (2021) - Early Cretaceous compressive structures in the Nansha block (Dangerous Grounds): Implications for the late Mesozoic tectonic regime on the southern margin of the South China Sea. Journal of Asian Earth Sciences, 222, 104963, https://doi.org/10.1016/j.jseaes.2021.104963.

Zhu W., Cui Y., Shao L., Qiao P., Yu P., Pei J., Liu X. & Zhang H. (2021) - Reinterpretation of the northern South China Sea pre-Cenozoic basement and geodynamic implications of the South China continent: constraints from combined geological and geophysical records. Acta Oceanologica Sinica, 40, 13-28, https://doi.org/10.1007/s13131-021-1757-7.

Zwaan F., Corti G., Keir D. & Sani F. (2020) - Analogue modelling of marginal flexure in Afar, East Africa: Implications for passive margin formation. Tectonophysics, 796, 228595, https://doi.org/10.1016/j.tecto.2020.228595.

Accepted manuscript